Review

Current understanding of the global cycling of carbon dioxide, methane, and nitrous oxide

By Takakiyo NAKAZAWA[*1,†]

(Edited by Taroh MATSUNO, M.J.A.)

Abstract: To address the climate change caused by anthropogenic emissions of greenhouse gases into the atmosphere, it is essential to understand and quantitatively elucidate their cycling on the Earth's surface. This paper first presents an overview of the global cycling of three greenhouse gases, carbon dioxide (CO_2), methane (CH_4), and nitrous oxide (N_2O), followed by a description of their variations in the atmosphere. This paper then presents the recent global budgets of these greenhouse gases estimated using two different approaches, top-down and bottom-up. Discussions on our current knowledge regarding the global cycling of the three gases are also presented.

Keywords: greenhouse gas, carbon dioxide, methane, nitrous oxide, global cycling, climate change

1. Introduction

The Earth's atmosphere has greatly changed since its birth 4.6 billion years ago. The present atmosphere consists mainly of nitrogen (N_2; approximately 78.084% by volume of dry air), oxygen (O_2; 20.947%), and argon (Ar; 0.934%). It also contains other constituents such as water vapor (H_2O; variable), carbon dioxide (CO_2; 0.04%), methane (CH_4; 0.0002%), and nitrous oxide (N_2O; 0.00003%). Because these constituents are almost transparent to solar radiation while strongly absorbing terrestrial radiation, they play an important role in producing the greenhouse effect, by which the global average surface temperature is raised by 33 °C to the observed value of about 15 °C. Thus, owing to their role in producing the greenhouse effect, the aforementioned atmospheric constituents are called "greenhouse gases".

It is known from the analyses of the air occluded in polar ice cores that the atmospheric burden of greenhouse gases fluctuated on timescales of glacial–interglacial cycles due to the changes in the Earth's orbital parameters.[1)–3)] It is also evident from polar ice core analyses and atmospheric observations[4)–9)] that CO_2, CH_4, N_2O, and other minor greenhouse gases, such as halocarbons and sulfur hexafluoride, have increased rapidly due to human activities. Such an increase would enhance the greenhouse effect and consequently change the state of climate globally. Global climate change (or "global warming") is one of the most serious global environmental problems encountered today. The Fifth Assessment Report of the Intergovernmental Panel on Climate Change (IPCC)[10)] summarized our current scientific knowledge and showed that the global average surface temperature rose by about 0.85 °C from 1880 to 2012 and that its main cause is attributable to the increase in atmospheric greenhouse gases emitted by human activities.

Global warming is not just about the rise in surface temperature but also about the changes in the entire global climate system and poses a threat to the whole biosphere. To cope with this human-induced global climate change, it is important to predict future climate change based on our present knowledge of the global cycling of greenhouse gases. We can thereby estimate the future permissible emissions of greenhouse gases for the given climate stabilization targets to mitigate excessive radiative forcing by greenhouse gases. To achieve this objective, we need to understand in detail the spatiotemporal variations in atmospheric greenhouse gases and their related

[*1] Tohoku University, Sendai, Miyagi, Japan.
[†] Correspondence should be addressed: T. Nakazawa, Center for Atmospheric and Oceanic Studies, Graduate School of Science, Tohoku University, Sendai, Miyagi 980-8578, Japan (e-mail: nakazawa@tohoku.ac.jp).

doi: 10.2183/pjab.96.030

variables and quantitatively estimate the budgets of anthropogenic greenhouse gases based on this knowledge. Considerable efforts have been devoted to a better understanding of the global cycling of the gases not only by performing comprehensive observations using various platforms and tools but also by employing top-down and bottom-up approaches based on various types of models and data.

By analyzing the atmospheric CO_2 data obtained using chemical measurement methods, G. S. Callendar claimed for the first time that atmospheric CO_2 increased in the first half of the 20th century due to fossil fuel combustion, causing the surface temperature to rise.[11] After his study, C. D. Keeling (Scripps Institution of Oceanography) began to systematically measure atmospheric CO_2 at the South Pole in 1957 and Mauna Loa, Hawaii, in 1958 using a modern high-precision instrument called non-dispersive infrared analyzer.[4),5)] Similar systematic observations were also started by the scientists at Stockholm University, Sweden, the National Oceanic and Atmospheric Administration (NOAA), U.S.A., the Commonwealth Scientific and Industrial Research Organisation (CSIRO), Australia, Environment Canada (the current Environment and Climate Change Canada), Canada, and Tohoku University, Japan in the 1960s–1970s. Systematic observations were also initiated for CH_4,[12),13)] N_2O,[14)] and halocarbons[8),15)] around 1980. Currently, similar observations are being conducted at 100–150 places around the world, using *in situ* continuous measurement methods and sampling of air in flasks with subsequent laboratory analysis. In addition to these ground-based stations, aircraft, ships, balloons, and satellites are also used as part of the overall global network of observations.[16)–22)]

Analysis of polar ice cores also began in the 1980s to reconstruct the past variations in atmospheric greenhouse gases.[23)] Quantitative studies on the global budgets of greenhouse gases were initially conducted for CO_2[24)–26)] and then for CH_4 and N_2O.[27)–29)] These studies have made considerable progress since the 2000s through the development of various types of models and the enrichment of related data.

This paper outlines our understanding of the global cycling of three greenhouse gases, namely, CO_2, CH_4 and N_2O, and then describes their observed spatiotemporal variations in the atmosphere, along with some recent estimates of their global budgets. Further, this paper discusses the activities that must be performed to better understand the global cycling of these gases. A similar review has been extensively conducted five times by the IPCC since 1991, but this paper concisely summarizes our current knowledge on global cycling, including the results obtained after the Fifth Assessment Report was published in 2013.

2. Global cycling of carbon dioxide, methane, and nitrous oxide

Figure 1 shows the conceptual illustration of the global cycling of CO_2, CH_4, and N_2O. There are four major carbon reservoirs on the Earth's surface, *i.e.*, the atmosphere, terrestrial biosphere, ocean, and geological reservoir. Carbon is exchanged as CO_2 between the atmosphere and terrestrial biosphere or ocean on timescales ranging from hourly to millennial, and carbon exchanges with geological reservoirs, such as limestone ($CaCO_3$), occur on longer timescales. These exchanges among the four carbon reservoirs constitute an essential aspect of the carbon cycle. Carbon is stored as gaseous CO_2 in the atmosphere, as organic matter in the terrestrial biosphere, and as dissolved inorganic carbon (DIC) (CO_2, HCO_3^-, and CO_3^{2-}, which are related by the chemical equilibria $CO_2 + H_2O \rightleftarrows H^+ + HCO_3^- \rightleftarrows 2H^+ + CO_3^{2-}$) or dissolved organic carbon (DOC) in water. The carbon exchange with the terrestrial biosphere is mainly governed by photosynthesis and respiration, including the oxidation of organic matter in soil, ($6CO_2 + 6H_2O \rightleftarrows C_6H_{12}O_6 + 6O_2$), and the exchange with the ocean can be attributed to the difference between the partial pressures of CO_2 in the surface ocean ($pCO_{2,sea}$) and the atmosphere ($pCO_{2,air}$) ($\Delta pCO_2 = pCO_{2,sea} - pCO_{2,air}$). There is also a small but persistent natural carbon flow, wherein organic carbon originating from the terrestrial biosphere and HCO_3^- produced by rock weathering on land are transported to the ocean by rivers and are then emitted into the atmosphere as CO_2 or accumulate as sediments on the sea floor.[30)] These exchange processes are affected by climate change induced, for example, by the changes in the Earth's orbital parameters (eccentricity, obliquity, and precession), the El Niño–Southern Oscillation (ENSO) events and volcanic eruptions. Thus, the atmospheric CO_2 level fluctuated even in times when the influence of anthropogenic emissions was negligibly small.

The global carbon cycle has altered because of a large amount of CO_2 emitted into the atmosphere by human activities, especially after the Industrial Revolution in the late 18th century.[31)] Its main sources are the combustion of fossil fuels such as coal,

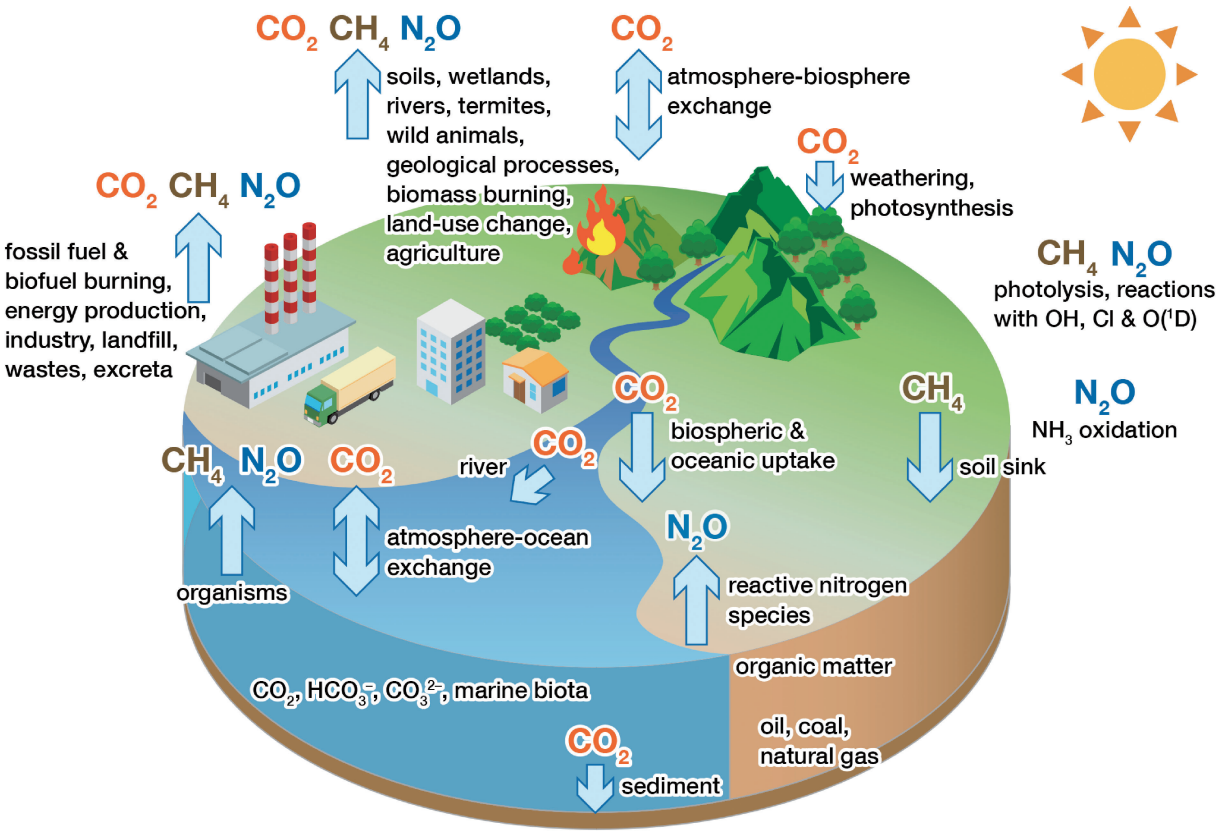

Fig. 1. Conceptual illustration of the global cycling of CO_2, CH_4, and N_2O.

oil, and natural gas ($C_xH_y + (x + y/4)O_2 \rightarrow xCO_2 + (y/2)H_2O$), and man-made changes in land use such as deforestation and cultivation. A small amount of CO_2 is also released into the atmosphere through cement production ($CaCO_3 \rightarrow CaO + CO_2$). The global carbon cycle is also affected by the changes in the CO_2 exchange between the atmosphere and terrestrial biosphere or ocean. Atmosphere–land CO_2 fluxes have been changed by the CO_2 fertilization effect caused by the increase in atmospheric CO_2, forest regrowth and reforestation. Atmosphere–ocean CO_2 fluxes due to the CO_2 partial pressure difference have been enhanced by the increased atmospheric CO_2, and ocean warming and ocean acidification have worked to decrease the fluxes. Both the atmosphere–ocean and atmosphere–land exchange processes would also have been affected by possible climate change over the past 100 years to some extent, and the magnitude of the exchange is likely to increase in the future. Some of anthropogenic CO_2 emitted into the atmosphere is absorbed by the ocean and terrestrial biosphere, and the rest remains in the atmosphere. Therefore, we must achieve sufficient quantitative understanding of the processes that govern the partitioning of CO_2 among these major carbon reservoirs under climate change (*i.e.*, climate change–carbon cycle feedback effect) to predict the future atmospheric CO_2 levels with a high degree of confidence.

CH_4 emissions are classified into three categories, namely, biogenic, thermogenic, and biomass burning, based on their production processes.[32),33)] CH_4 is emitted naturally into the atmosphere from wetlands, rivers, wild animals, termites, wildfires, geological processes, and oceans. CH_4 is also released from anthropogenic sources such as consumption and production of fossil fuels, biomass and biofuel burning, ruminants, landfills, wastes, rice cultivation, and manure. On the other hand, CH_4 is destroyed primarily via chemical reaction with OH in the troposphere and partly via reactions with OH, $O(^1D)$, and Cl in the stratosphere ($CH_4 + OH \rightarrow CH_3 + H_2O$, $CH_4 + O(^1D) \rightarrow OH + CH_3$, and $CH_4 + Cl \rightarrow HCl + CH_3$). Thus, because OH is produced by $O_3 + h\nu$ (UV) $\rightarrow O_2 + O(^1D)$ and $O(^1D) + H_2O \rightarrow 2OH$, the destruction of CH_4 becomes the maximum

in summer. There are two additional small CH_4 sinks, *i.e.*, methanotrophic bacteria in soils and reaction with Cl in the marine atmospheric boundary layer. The atmospheric CH_4 level is determined by the balance of the source and sink strengths, and its variations are considerably affected by the changes in both these variables because the lifetime of CH_4 in the atmosphere is relatively short, *i.e.*, about 9 years.[32),34)]

N_2O is a long-lived gas with an atmospheric lifetime of about 120 years,[34)–36)] because this gas is very stable in the troposphere and destroyed only in the stratosphere through photolysis by ultraviolet light and chemical reactions with $O(^1D)$ ($N_2O + h\nu \rightarrow N_2 + O(^1D)$, $N_2O + O(^1D) \rightarrow 2NO$, and $N_2O + O(^1D) \rightarrow N_2 + O_2$), and the contributions to the destruction are approximately 90%, 6%, and 4%, respectively.[37)] N_2O is produced naturally via the microbial metabolic processes of nitrification under aerobic conditions ($NH_4^+ \rightarrow NH_3 \rightarrow NH_2OH \rightarrow NO_2^- \rightarrow NO_3^-$, $NH_2OH \rightarrow N_2O$) and denitrification under anaerobic conditions ($NO_3^- \rightarrow NO_2^- \rightarrow NO \rightarrow N_2O \rightarrow N_2$) in the soil and ocean, and via the oxidation of NH_3 in the atmosphere ($NH_3 + OH \rightarrow NH_2 + H_2O$, $NH_2 + NO_2 \rightarrow N_2O + H_2O$).[38),39)] Anthropogenic N_2O is produced by fossil fuel combustion, industrial processes (mainly nylon and nitric acid production), agricultural activities such as the usage of nitrogenous and organic fertilizers, biomass and biofuel burning, human excreta, and the deposition of reactive nitrogen species on the land and ocean.[39)] Due to the long life of N_2O in the atmosphere, its atmospheric level on timescales ranging from a few decades to hundreds of years is more effectively affected by changes in emission rather than in destruction.

3. Variations in carbon dioxide, methane, and nitrous oxide in the atmosphere

As expected from the abovementioned source/sink processes, atmospheric CO_2, CH_4, and N_2O are quite variable in time. They also exhibit spatial variability characterized by the presence of unevenly distributed sources and sinks on the Earth's surface. In this section, the spatiotemporal variations in the three gases are concisely described.

3.1. Glacial–interglacial variations. As mentioned above, atmospheric CO_2, CH_4, and N_2O vary in response to the naturally occurring changes in the climate system. The most striking variation observed on the one-million-year timescale is the glacial–interglacial cycle that is spectrally consistent with the changes in the Earth's orbital parameters, as shown in Fig. 2.[3)] The results shown in the figure were obtained by analyzing the air occluded in deep ice cores collected from Dome C and Vostok in Antarctica. The atmospheric abundance (in units of dry air mole fraction) fluctuates between 180 ppm during the glacial maximum and 280 ppm during the interglacial period for CO_2 and between 350 and 700 ppb in the corresponding periods for CH_4. The N_2O data are considerably scattered during the glacial period, probably due to N_2O produced in the Antarctic ice sheet by microbes transported from the continents. However, the mole fraction values appear to be lower in the glacial period than in the interglacial period.

To interpret the low CO_2 mole fractions during the glacial period, several hypotheses have been proposed. As can be understood from Fig. 1, we need to enhance the terrestrial biospheric and/or oceanic CO_2 uptake to lower the atmospheric CO_2 level. However, the enhancement of the terrestrial biospheric uptake would be a minor effect because the weather was cool and dry, solar radiation was reduced, and northern mid- and high-latitude continents with a large quantity of terrestrial biomass were covered by ice and snow in the glacial period. The isotope analyses of benthic foraminifera in the ocean floor sediments indicated that the carbon isotope ratio ($\delta^{13}C$), which will be defined in Section 3.2, was decreased by 0.03‰–0.04‰ in the glacial period, suggesting that there was an inflow of isotopically light biospheric carbon of 300–700 GtC from land.[40)] Therefore, the oceanic CO_2 uptake is the remaining major mechanism by which atmospheric CO_2 decreased during the glacial period. For this mechanism to work, the surface ocean CO_2 partial pressure needs to be lower than the atmospheric CO_2 partial pressure, and several potential processes have been proposed to achieve this. The surface ocean CO_2 partial pressure can be reduced by (1) increasing the CO_2 solubility of seawater because of decreasing temperature, (2) enhancing the marine biospheric activities by increased supply of nutrients, and/or (3) increasing the alkalinity of seawater because of changes in the ocean carbonate chemistry.[41)–44)] It is also known that there is a good correlation between the atmospheric CO_2 mole fraction and Antarctic air temperature. Based on this correlation, several studies have ascribed the cause to the Southern Ocean, *i.e.*, the enhancement of marine biospheric activities by the increased supply of Fe from the continents under dry and

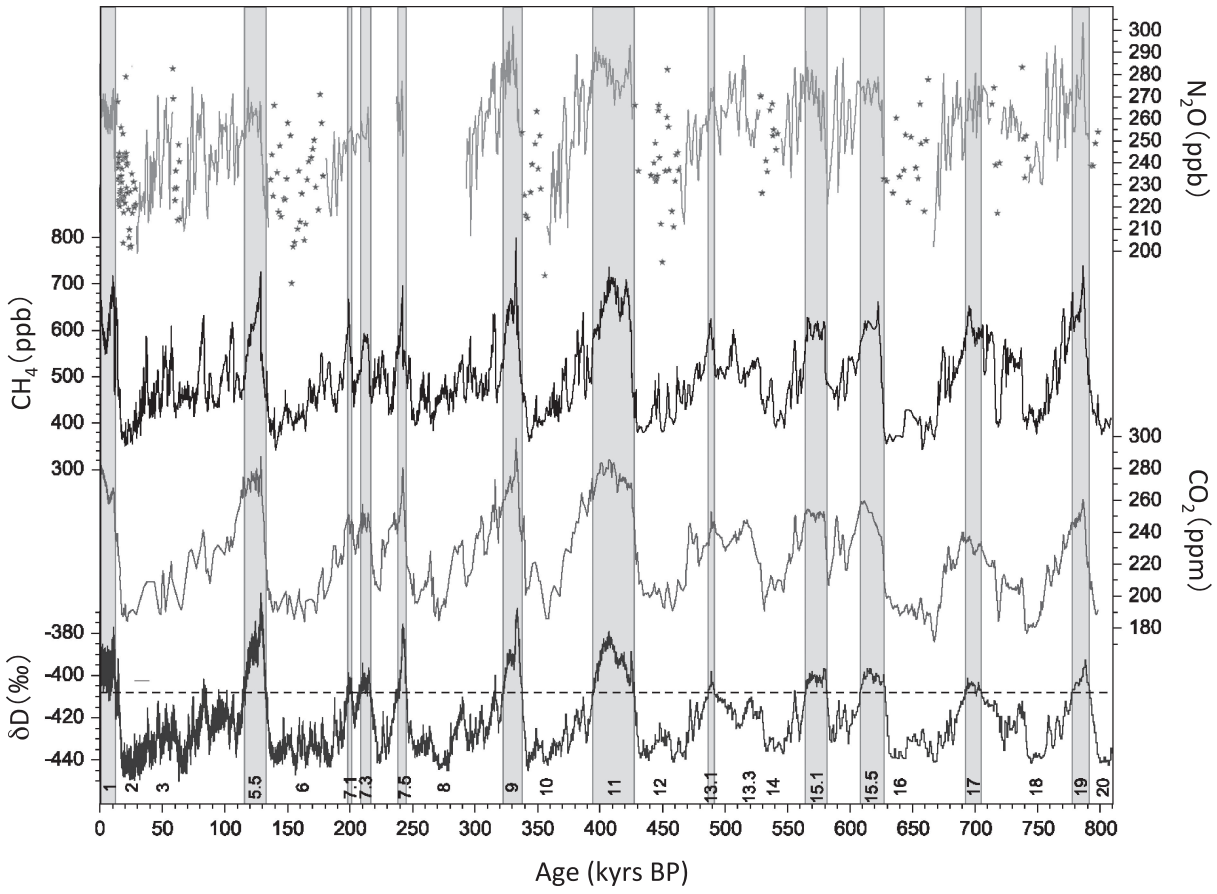

Fig. 2. Variations of atmospheric CO_2, CH_4, and N_2O and δD_{ice} obtained from the deep Antarctic ice cores (Schilt *et al.*[3]). The stars plotted for N_2O represent the data that could have been affected by N_2O produced in the ice sheet. The numbers in the lowermost part of the figure indicate the marine isotope stage, and the vertically shaded bars denote the interglacial periods.

windy weather conditions and the suppression of CO_2 release due to the weakened upwelling of seawater by northward movement of the westerly wind zone or due to the expanded sea ice.[45)–47)] Despite these previous studies, our knowledge of the paleocarbon cycle is still insufficient to conclude with certainty the process that played a more definitive role in reducing the glacial atmospheric CO_2 mole fraction. However, it seems likely that all the processes identified above worked in combination to some extent to make an overall contribution.

To explain the low glacial atmospheric CH_4 levels, both the decrease in emission and increase in sink should be considered. In the glacial period with cool and dry weather conditions and reduced solar radiation, the production of OH from H_2O would have decreased, leading to a reduction in CH_4 destruction. On the other hand, the emission of non-methane volatile organic compounds (NMVOCs), which react easily with OH, was considerably reduced due to the fact that northern mid- and high-latitude forests were covered by snow. In this regard, Levine *et al.*[48)] used a global atmospheric chemistry model to report that both the effects (decrease in OH production and NMVOC emissions) offset each other. Murray *et al.*[49)] also suggested that the tropospheric OH levels in the last glacial maximum and in the pre-industrial era were similar. Soil sinks are expected to be almost unchanged in these two periods, because boreal forests decreased while low-latitude deserts expanded in the last glacial maximum.[50)] Based on these results, the observed low glacial CH_4 mole fractions can only be attributed to the reduction in CH_4 emissions. The strongest natural CH_4 source is wetlands. Based on the restoration of vegetation distributions and model analysis, it is suggested that global wetlands have halved in the last glacial maximum and that their

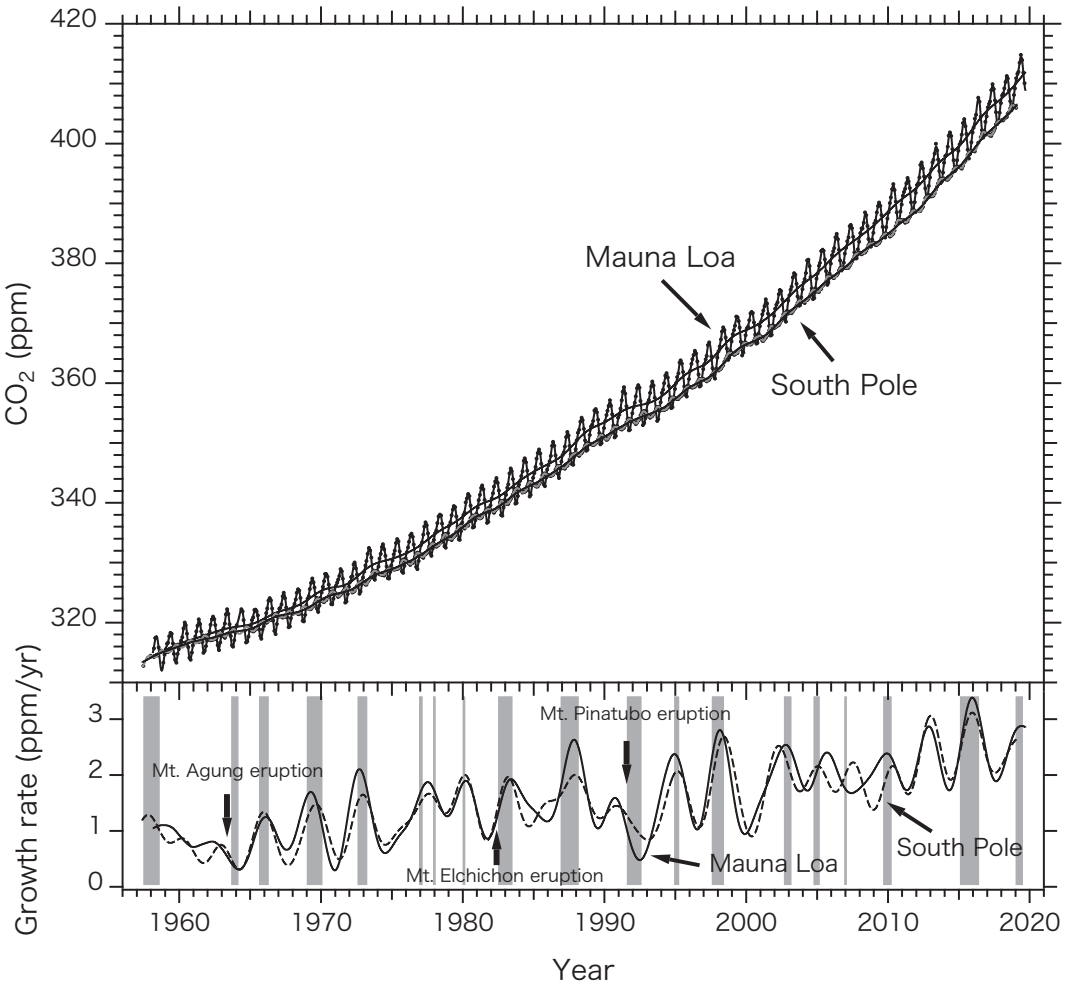

Fig. 3. Variations in the mole fraction (upper panel) and growth rate (lower panel) of atmospheric CO_2 at Mauna Loa, Hawaii and the South Pole. The smooth lines in the upper panel show a long-term trend, and the shaded vertical bars in the lower panel represent El Niño occurrences.

CH_4 emissions have decreased by 40% compared with the values in the pre-industrial Holocene.[50),51)]

It is not easy to exactly estimate the past lifetime of atmospheric N_2O, but some model studies show that the lifetime varied within ±15% from the last glacial maximum to the present time, or that the lifetime is slightly longer during the glacial period than at the present time.[34),52),53)] If this is true, the low glacial N_2O levels are primarily ascribed to the reduction in N_2O emissions. From the analyses of Antarctic ice cores for N_2O and its nitrogen and oxygen isotope ratios, it is reported that the N_2O emission was reduced by 30%–40% around the time of the last glacial maximum compared to the pre-industrial Holocene values, with nearly equal contributions from soils and oceans.[54),55)]

3.2. Human-caused increase superimposed on natural variations.

3.2.1. Carbon dioxide. Figure 3 shows the temporal variations of atmospheric CO_2 at the South Pole and Mauna Loa.[56)] It also shows the long-term trends and growth rates derived using a digital filtering technique,[57)] El Niño periods, and volcanic eruptions. It is clearly seen that atmospheric CO_2 increased over time, accompanied by a seasonal cycle and interannual variations with periods of a few or several years. The yearly mean CO_2 mole fraction increased from 314–315 ppm in 1958 to 403–407 ppm in 2017, indicating a time-dependent growth rate from 1.0 ppm/yr during 1958–1960 to 2.6 ppm/yr during 2015–2017.

The seasonal CO_2 cycle can be mainly attributed

to the seasonally dependent CO_2 exchange between the atmosphere and terrestrial biosphere. Under the present condition, the $\delta^{13}C$ of atmospheric CO_2, which is expressed as

$$\delta^{13}C = \left[\frac{(^{13}C/^{12}C)_{sample}}{(^{13}C/^{12}C)_{standard}} - 1 \right] \times 1000\ (‰), \quad [1]$$

where the subscripts "sample" and "standard" represent the sample and international standard, respectively, is affected by $-0.05‰$/ppm due to the CO_2 exchange between the atmosphere and terrestrial biosphere and by $-0.003‰$/ppm due to the exchange between the atmosphere and ocean. The observed seasonal cycles of atmospheric CO_2 and its $\delta^{13}C$, especially in the northern hemisphere, yield about $-0.05‰$/ppm, suggesting the cause to be the atmosphere–terrestrial biosphere CO_2 exchange.[16),17)] Therefore, the seasonal amplitude is larger at Mauna Loa than at the South Pole, reflecting the hemispheric difference in the terrestrial biomass, and the seasonal phases at the two stations are the opposite.

The interannual CO_2 variations superimposed on the observed long-term upward trend correlate well with the El Niño events that generally result in high temperatures and dry conditions in many areas of the world, especially in the tropics. From the results of the Atmospheric Tracer Transport Model Intercomparison Project (TransCom) flux inversion calculations based on global atmospheric transport models constrained by the atmospheric CO_2 observations,[39)] as shown in Fig. 4, the CO_2 exchange between the atmosphere and terrestrial biosphere is considerably affected by the occurrence of an El Niño event. This implies that a large amount of terrestrial biospheric CO_2 is emitted into the atmosphere through the enhanced respiration of plants, the accelerated decomposition of organic matter on/in soils, droughts, and forest fires. This idea is also supported by the $\delta^{13}C$ observations.[16),17)]

The interannual variations in the atmosphere–terrestrial biosphere CO_2 fluxes exhibited negative values during a few years after the eruption of Mt. Pinatubo, Philippines, in June 1991, although an El Niño event occurred at the same time. As a result of the volcanic eruption, large amounts of sulfate aerosols were produced in the stratosphere, reducing the amount of direct solar radiation reaching the surface and the surface temperature. This reduced the terrestrial biosphere respiration while enhancing photosynthesis by greater diffused radiation at the canopy level. On the other hand, it is evident from Fig. 4 that the CO_2 fluxes between the atmosphere and ocean show smaller temporal variability than those between the atmosphere and terrestrial biosphere, although some inversion studies have shown an enhancement in oceanic sink during strong El Niño events, for example, in 1997–1998.[58),59)] As shown in Fig. 3, low growth rates are associated with the eruption of Mt. Agung, Indonesia, in March–May 1963, but an opposite situation could be observed after the eruption of Mt. El Chichón, Mexico, in March 1982 when the growth rate increased. The latter situation is likely due to the possibility that the El Niño effect overwhelmed the volcanic eruption effect.

Figure 3 indicates that the yearly mean CO_2 mole fraction is always higher at Mauna Loa than at the South Pole and that the difference between the two stations has gradually expanded with time from 0.5 ppm at the beginning of the observation to 3.7 ppm during 2013–2017. The observed north–south difference implies that the CO_2 sources (sinks) exist in the northern (southern) hemisphere and that their strength is enhanced over time. Considering the fact that atmospheric CO_2 has increased rapidly since the late 1950s, the north–south difference can be attributed to the northern hemispheric sources, *i.e.*, fossil fuel consumption. 95% of fossil fuels are currently consumed in the northern hemisphere.

To understand the global carbon cycle, it is important to know the variations in atmospheric CO_2 before the modern systematic observations were conducted. Therefore, considerable efforts have been devoted to reconstruct the past CO_2 levels using various methods. Among these methods, the analysis of polar ice cores drilled at sites with high snow accumulation rates was the most promising. Figure 5 shows the variations of atmospheric CO_2, CH_4, and N_2O over the past 300 years obtained from the analysis of an ice core collected at H15, Antarctica and the yearly mean values observed in the atmosphere at the South Pole or Cape Grim, Australia.[6),8),56),60),61)] The CO_2 mole fraction remained almost constant at approximately 280 ppm in the mid-18th century, and it increased gradually until the mid-20th century and then quite rapidly thereafter toward the present level. The overall increase between the mid-18th century and present time amounted to more than 120 ppm, which is larger than the interglacial–glacial difference of about 100 ppm. Similar variations were also observed in other Antarctic ice cores.[9)] The air samples extracted from the ice cores were measured for obtaining the $\delta^{13}C$ of CO_2.[9),62)] Results show that $\delta^{13}C$ decreased gradually

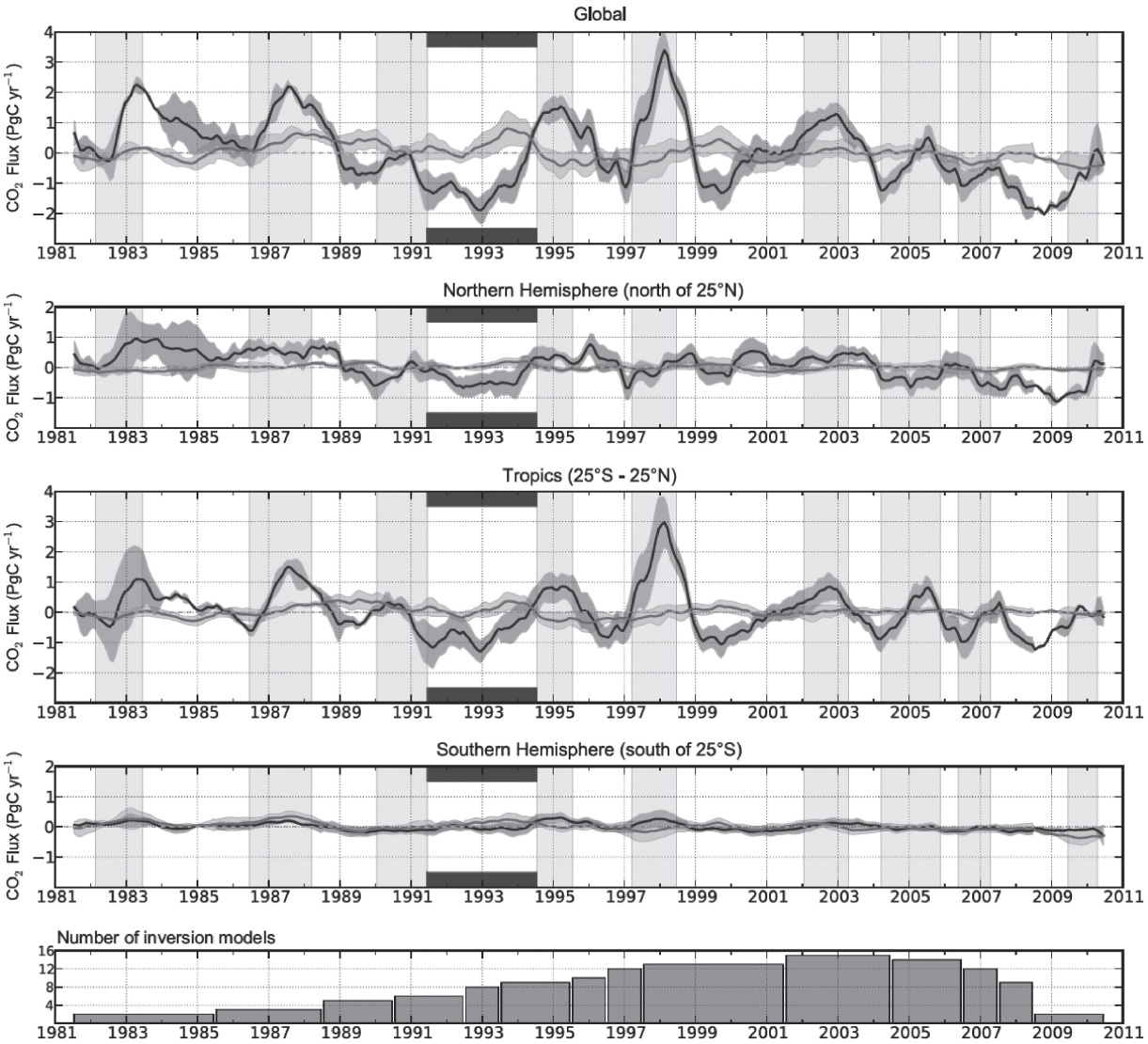

Fig. 4. The atmosphere–ocean (gray lines) and atmosphere–terrestrial biosphere (black lines) fluxes of CO_2 estimated by the TransCom flux inversion calculations for the global, northern (north of 25°N), tropical (25°N–25°S), and southern (south of 25°S) areas (Ciais *et al.*[39]). The occurrences of El Niño are indicated by the lightly shaded vertical bars in each of the upper four panels, and the heavily shaded bars indicate the low-temperature period after the eruption of Mt. Pinatubo in 1991. The lowest panel shows the number of models used for atmospheric inversion.

from −6.4‰ at around 1750 to −7.0‰ at around 1950 and then rapidly to −7.8‰ at around 1980. The trend of $\delta^{13}C$ is similar to that of CO_2 but with an opposite sign. The observed good correlation between CO_2 and $\delta^{13}C$ suggests that the long-term CO_2 increase over the last 250 years was mainly caused by emissions of isotopically light CO_2 into the atmosphere via fossil fuel combustion (−27‰) and/or land-use change/deforestation (−25‰). The CO_2 released from or taken up by the ocean (0‰–2‰) has very little influence on atmospheric $\delta^{13}C$ because the kinetic isotope fractionation factors for the ocean-to-atmosphere and atmosphere-to-ocean CO_2 exchange flows are different. Therefore, the $\delta^{13}C$ values of CO_2 added to and removed from the atmosphere are close to the atmospheric $\delta^{13}C$.[16),17)] The atmospheric $\delta^{13}C$ value continued to decrease until its global average reached −8.5‰ in the mid-2010s.[63)]

3.2.2. Methane. As shown in Fig. 5, atmospheric CH_4 was about 700 ppb in the early 1700s. Similar values have also been obtained using other Antarctic ice cores.[9)] On the other hand, the ice cores from

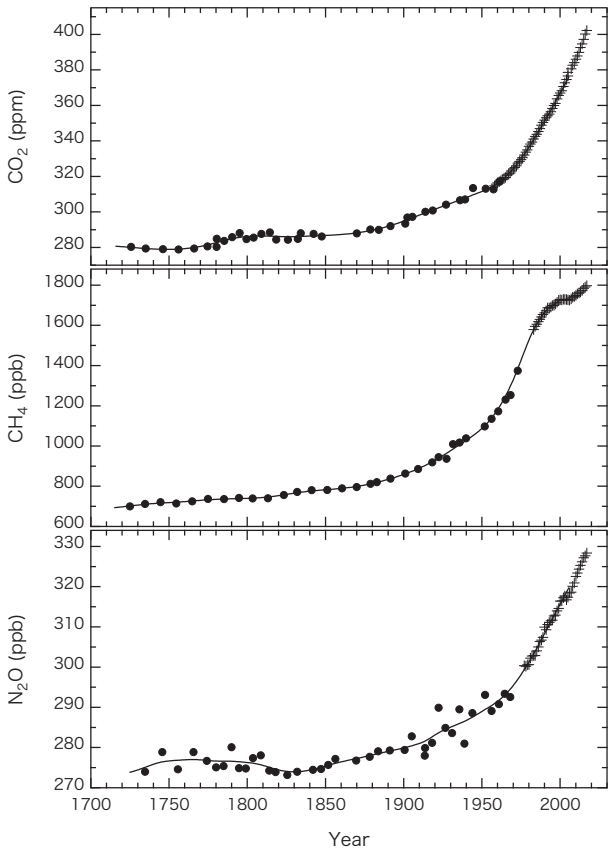

Fig. 5. Variations of atmospheric CO_2, CH_4, and N_2O reconstructed from the shallow Antarctic ice core, H15 (circles). The yearly means obtained from the systematic observations at the South Pole are also plotted for CO_2 and CH_4, and the values at Cape Grim, Australia, are plotted for N_2O (crosses).

Greenland indicate higher pre-industrial CH_4 values by 30–50 ppb when compared with those from Antarctica due to natural CH_4 emissions from boreal wetlands.[9),64),65)] It can be observed from Fig. 5 that the Antarctic CH_4 mole fraction increases constantly from the pre-industrial levels to the present value of about 1790 ppb, with the increase being more than three times the interglacial–glacial difference of 350 ppb.

To examine the temporal variations in atmospheric CH_4 in detail, the globally-averaged monthly mean values obtained by the NOAA/Earth System Research Laboratory (ESRL)/Global Monitoring Division (GMD)[6)] are plotted in Fig. 6 along with the best-fit curve, long-term trend, and growth rate. Similar to CO_2, atmospheric CH_4 shows a seasonal cycle, interannual variations, and a long-term increase. The seasonal CH_4 cycle is a combined effect of the seasonally varying sources and sinks. Because the major sink of CH_4 is the reaction with OH, its destruction is maximized during summer. The seasonality of CH_4 emission is dependent on individual sources. For example, the CH_4 emissions from wetlands and fossil fuel burning are enhanced in warm and cold seasons, respectively. However, because the seasonal CH_4 minimum is observed in summer under baseline conditions, the sink effect takes precedence over the source effect. The observed interannual variations of atmospheric CH_4 are caused by the ENSO events and volcanic eruptions. For example, a large amount of CH_4 is released into the atmosphere through increased biomass burning under dry conditions during the El Niño event and increased tropical land precipitation during the La Niña event. High growth rates can be found even with respect to the globally averaged CH_4 mole fractions shown in Fig. 6, especially during El Niño. The CH_4 emissions from wetlands associated with the ENSO events and from the El Niño-related Indonesian fires were examined by various researchers, including Hodson *et al.*[66)] and Worden *et al.*[67)] Figure 6 indicates that the growth rate of CH_4 is increased just after the eruption of Mt. Pinatubo in 1991 and decreased considerably thereafter. This can be attributed to attenuated ultraviolet actinic flux in the 290–310 nm wavelength range due to the absorption by SO_2 injected into the stratosphere and perturbed ultraviolet flux by sulfate aerosols produced from SO_2, and to decreased CH_4 emissions from boreal wetlands due to low temperatures after the eruption.[68)]

Figures 5 and 6 indicate that the atmospheric CH_4 trend has behaved in an unexpected manner in the last few decades. It rose rapidly until 1991 and gradually from 1991 to 1999, leveled off in 1999–2006, and then increased again. By inspecting the CH_4 data in the north and south polar regions, Dlugokencky *et al.*[69)] found that the average difference between the two regions was 140 ppb during 1984–1991, which is 3–5 times larger than the pre-industrial values probably due to human activities at northern mid- and high latitudes. It was also found that the difference decreased suddenly in 1992 and then gradually reduced with time until 2001. The decreasing interpolar difference and the decelerating CH_4 growth in the 1990s would have resulted from a reduction in the fossil-fuel CH_4 emissions associated with the collapse of the former Soviet Union and a reduction in leakage during natural gas and oil production and their transportation owing to subsequent facility improvements.[6),69),70)] Atmospheric

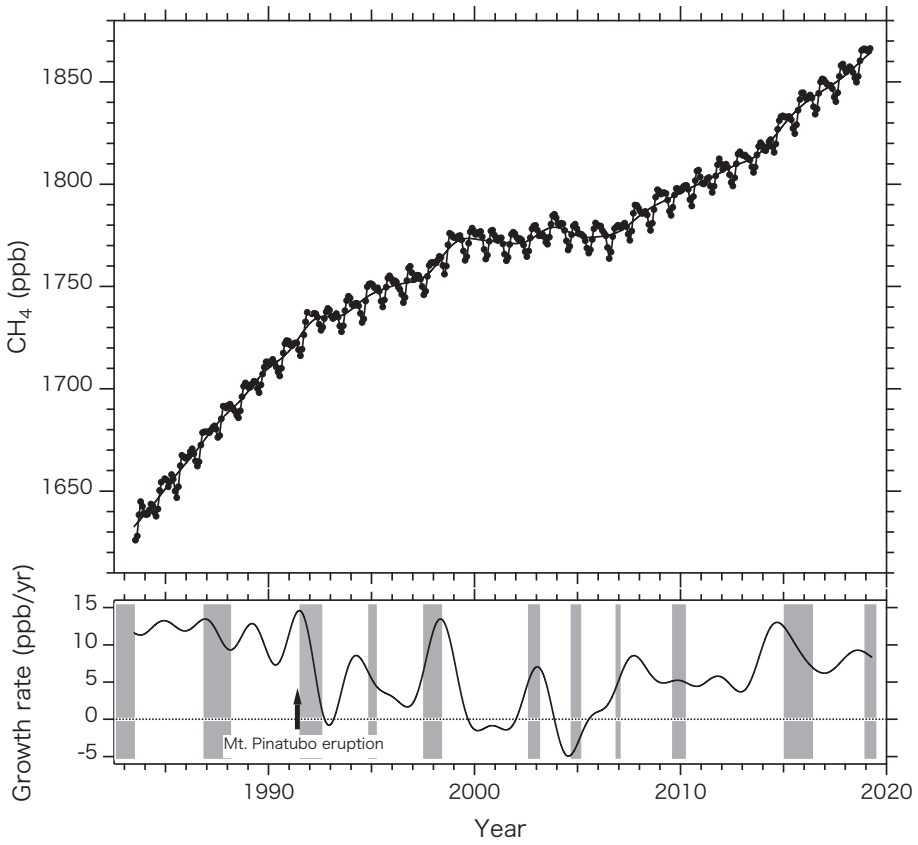

Fig. 6. Globally averaged monthly means of the atmospheric CH_4 mole fraction (circles in the upper panel) and the growth rate (solid line in the lower panel). El Niño periods are indicated by shaded vertical bars. The best-fit curve to the observed data and the long-term trend are shown by solid lines in the upper panel.

CH_4 began to increase in 2007 and the trend continued until 2018. Because the observed $\delta^{13}C$ values of CH_4 indicate a gradual decrease after 2007,[71),72)] the isotopically light biogenic CH_4 sources would play an important role in the recent increase in the observed mole fraction.

To interpret the renewed increase of CH_4 from 2007, scientists have analyzed the variations of CH_4, $\delta^{13}C$, C_2H_6, or CH_3CCl_3 in the atmosphere. However, the cause is still under debate because there are large uncertainties not only in anthropogenic and natural sources but also in sinks.[69),71),73)–77)] As mentioned above, the atmospheric CH_4 burden is governed by the balance between emissions from various surface sources and destruction in the atmosphere, mainly by OH. However, it is impossible to derive a global OH concentration field from observations because its lifetime is very short, *i.e.*, a few seconds, and its tropospheric concentration is very low (in the order of 10^6 molecules/cm^3) and spatiotemporally variable.[78)] The calculation results obtained using the current atmospheric chemistry models are also diverse.[79)] The CH_4 sources are unevenly distributed on the Earth's surface, and their strengths are variable in time and space. Therefore, it is not easy to identify the process (or set of processes) that increased CH_4 after 2007. By assuming OH to be invariant with time in case of global inverse modeling calculation constrained by the atmospheric CH_4 observations, Patra *et al.*[73)] reported that the renewed CH_4 increase from 2007 was caused by the biogenic emissions in tropical Asia and southern South America. Nisbet *et al.*[71)] suggested from their analyses of atmospheric CH_4 and $\delta^{13}C$ that the CH_4 increase after 2007 can be attributed to the biogenic CH_4 emissions particularly in the tropics, for example, through the expansion of tropical wetlands by positive rainfall anomalies or enhanced emissions from agricultural sources such as ruminants and rice paddies. They also reported that the changes in the removal rate by OH appear to be a small effect. Thompson *et al.*[76)] proposed from their simultaneous

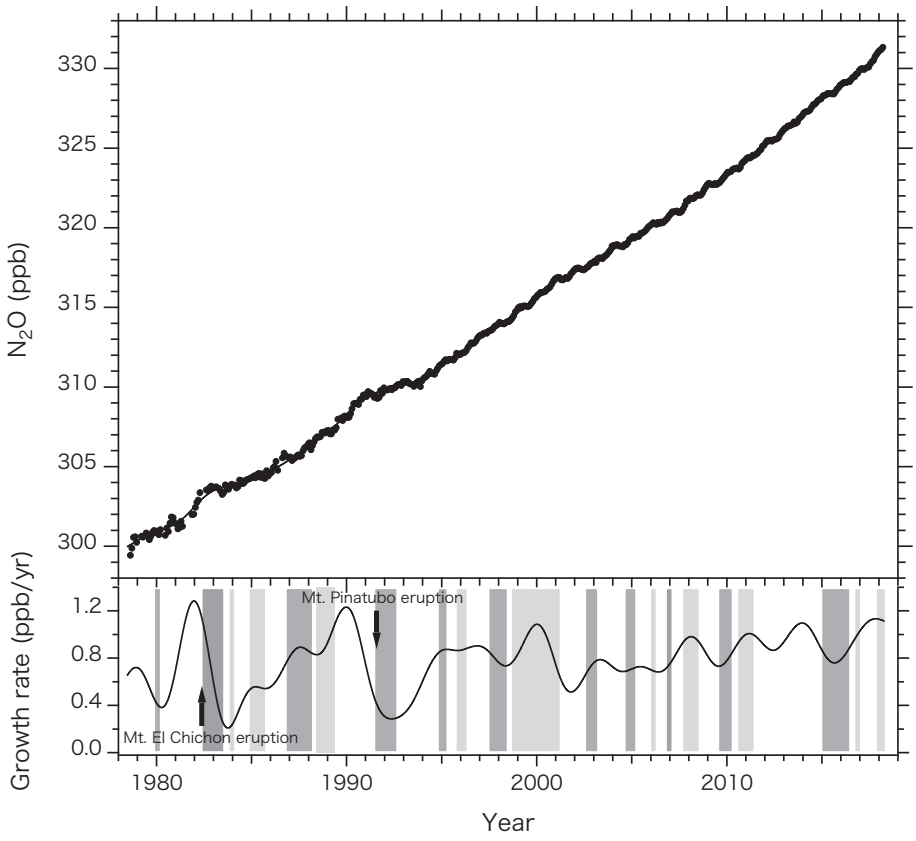

Fig. 7. Global averages of the atmospheric N_2O mole fraction (circles in the upper panel) and the growth rate (solid line in the lower panel). The solid line in the upper panel shows the long-term trend, and the dark and lightly shaded vertical bars in the lower panel represent the El Niño and La Niña periods, respectively.

analyses of CH_4, $\delta^{13}C$, and C_2H_6 that the biogenic and fossil-fuel CH_4 emissions were responsible for the CH_4 increase from 2007 and that the changes in the removal rate by OH do not appear to be a major factor. On the other hand, Rigby *et al.*[74] and Turner *et al.*[75] analyzed the observed trend of atmospheric CH_3CCl_3, the major sink of which is the reaction with tropospheric OH, using a box model inversion and reported that the global average OH concentration decreased from around 2003, resulting in the CH_4 increase after 2007. Naus *et al.*[77] identified biases in the two-box model approach based on the results of full three-dimensional transport model simulations and found that the tropospheric OH concentration increased gradually with time from 1994 to 2014 and that the CH_4 emissions increased from 2007. Further advanced studies are required to obtain a more definitive conclusion on the recent unexpected but interesting CH_4 trend.

3.2.3. Nitrous oxide. Figure 5 shows that atmospheric N_2O was approximately 275 ppb before the early 1800s and gradually increased from 1850 to 1960–1970 and then rapidly to about 328 ppb in 2017. The increase from the pre-industrial era to the present time is 53 ppb, indicating a 20% increase relative to the pre-industrial level. Similar variations were also reported from the analyses of other ice cores.[9]

The global average monthly mole fractions of atmospheric N_2O observed by the Advanced Global Atmospheric Gases Experiment (AGAGE) are shown in Fig. 7[8] along with the long-term trend and growth rate. Atmospheric N_2O also shows a seasonal cycle, interannual variations and a long-term increase. Because N_2O is very stable in the troposphere, the seasonal cycle and interannual variations would be closely related with the source activities and atmospheric transport. From the beginning of the atmospheric N_2O observations, the seasonal N_2O cycle has been difficult to detect, but a very small seasonality with a peak-to-peak amplitude of about 1 ppb was recently observed due to the improved measurement precision.[8),20] The cause of the seasonal

N_2O cycle is not fully understood yet. However, because the timing of the appearance of the seasonal maximum and minimum seems to depend on the location of the observation, the seasonal N_2O cycle is probably a result of the combination of some seasonally dependent processes such as, for example, troposphere–stratosphere air exchange, air transport in the troposphere, interhemispheric air mixing, N_2O production by bacteria, and N_2O exchange between the atmosphere and ocean. The N_2O mole fraction is lower in the stratosphere and southern hemisphere when compared with those in the troposphere and southern hemisphere, respectively, and bacterial activities in soils and oceans are seasonally dependent.[8),18),20),80)]

As shown in Fig. 7, the growth rate of N_2O is correlated with the occurrences of the El Niño and La Niña events, showing low values during the former and high values during the latter. It should be noted that the measurement precision is not the same throughout the period, but the good correlation can be interpreted as follows. Because the N_2O emissions from the soil and ocean amount to 60% of the total emissions and the anthropogenic N_2O emissions are considered to have very small year-to-year variations, such a correlation is likely to arise from the changes in N_2O emissions from natural sources. It is known that the soil moisture, temperature, and precipitation are especially important for N_2O production in soils. In general, the tropical and subtropical regions become hot and dry during El Niño and become cold and wet during La Niña. The oceanic N_2O emissions are reduced by the suppressed upwelling in the eastern tropical Pacific during El Niño. Therefore, the N_2O emissions from the soils and oceans at low latitudes would play an influential role with respect to the observed interannual variations of atmospheric N_2O. This idea is also suggested by terrestrial biogeochemical modeling, atmospheric chemistry/transport modeling and shipboard observations in the Pacific Ocean.[20),81),82)] The low N_2O growth rates observed after the eruptions of Mt. Pinatubo in 1991 and Mt. El Chichón in 1982 would be related to the decreased N_2O emissions from soils due to low temperatures, in addition to the El Niño effect.

Atmospheric N_2O increased from about 300 ppb in the late 1970s to the present value of 331 ppb, with an average growth rate of 0.78 ppb/yr. The average growth rates for 1979–1998 and 1999–2017 were 0.72 and 0.85 ppb/yr, respectively, implying that the N_2O increase was enhanced more in the latter period than in the former period. Weiss[14)] reported, based on their measurements in 1976–1980, that the average N_2O growth rate was about 0.5 ppb/yr, which is even lower than the value obtained during 1979–1998.

By analyzing the atmospheric N_2O data collected systematically by the NOAA/ESRL/GMD, AGAGE and Tohoku University, it is found that the average mole fraction is the lowest at the South Pole, increases by about 1 ppb toward the equator, increases by an additional 1 ppb toward the northern mid-latitudes, and then declines by 0.5 ppb in the northern polar region. This latitudinal N_2O distribution indicates the existence of N_2O sources in regions extending from the tropics to northern mid-latitudes.

4. Global budgets of anthropogenic carbon dioxide, methane, and nitrous oxide

Our understanding of the global budgets of anthropogenic greenhouse gases is based on two approaches: "top-down" in which fluxes are inferred by analyzing the atmospheric observations using global atmospheric chemistry/transport models, and "bottom-up" in which inventories, extrapolation of local flux observations, and process models are used to estimate the fluxes. Both these approaches have advantages and disadvantages. Time-dependent global and/or regional fluxes can be derived using the top-down approach even from short records of atmospheric observations under the constraint that budgets are balanced. However, this approach is often afflicted by the coarse resolution of the data obtained from the observation network, the biases in measurement owing to the participation of various institutes and the usage of various observation methods, and our insufficient knowledge on atmospheric transport and sinks. On the other hand, in the bottom-up approach, we can estimate various fluxes associated with each of the source and sink processes. However, this approach is seriously affected by the uncertainties and potential biases in the usable statistical data, conversion factors for emissions and extrapolation to geographically large scales from a limited number of observations. Various budgets estimated by the bottom-up approach are not constrained for balance, for example, by atmospheric observations. Therefore, to accurately evaluate the global greenhouse gas budget, it is important to achieve a scientifically consistent merger of the results obtained using these multifaceted approaches.[83)]

In this section, the global budgets estimated for anthropogenic CO_2, CH_4, and N_2O using the top-down and bottom-up approaches are presented and discussed.

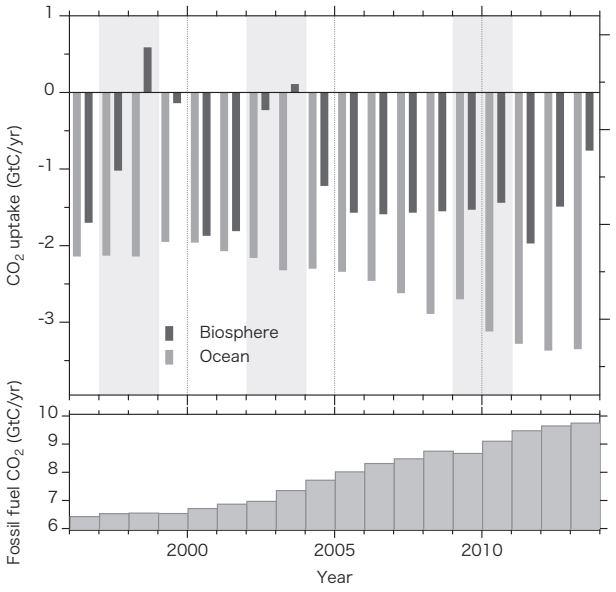

Fig. 8. Terrestrial biospheric and oceanic uptake of anthropogenic CO_2 estimated by the simultaneous analysis of atmospheric CO_2 and $\delta^{13}C$ (upper panel) and global fossil-fuel CO_2 emissions (lower panel) for 1996–2013 (Goto *et al.*[85]).

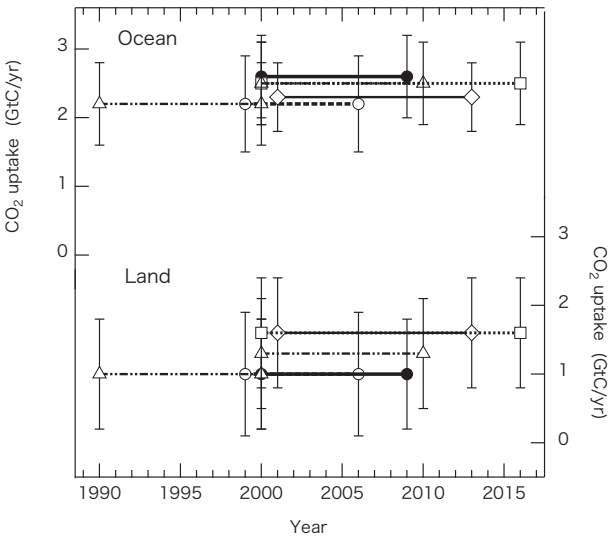

Fig. 9. Terrestrial biospheric and oceanic uptake of anthropogenic CO_2 estimated on the basis of atmospheric CO_2 and O_2. Open circles, solid circles, triangles, diamonds, and squares represent the respective results of Tohjima *et al.*,[87] Ishidoya *et al.*,[89] Keeling and Manning,[90] Goto *et al.*,[85] and Tohjima *et al.*[88]

4.1. Carbon dioxide. The global budget for CO_2 has been estimated using several methods. For example, Francey *et al.*[84] and Goto *et al.*[85] analyzed the atmospheric CO_2 mole fraction and its $\delta^{13}C$. The $\delta^{13}C$ values in the atmosphere, ocean and terrestrial biosphere are different, and the kinetic fractionation factors of CO_2 flow from the atmosphere to the terrestrial biosphere or ocean and vice versa are also different. Based on these isotope properties, the global net terrestrial biospheric and oceanic carbon fluxes can be estimated by simultaneously solving a set of mass balance equations for atmospheric CO_2 and $^{13}CO_2$. The CO_2 uptake inferred using the data obtained at Ny-Ålesund, Svalbard during 1996–2013 is presented in Fig. 8 along with the global fossil-fuel CO_2 emissions.[85] The average terrestrial biospheric and oceanic CO_2 uptake values over 18 years were 1.3 and 2.6 GtC/yr, respectively, which are relatively consistent with the results obtained based on atmospheric O_2 analyses that will be discussed below. It is also clearly shown in Fig. 8 that the terrestrial biosphere shows larger year-to-year variations in CO_2 uptake when compared with the ocean uptake, which are correlated with the occurrences of the El Niño events. However, there was no considerable decrease in the terrestrial biospheric CO_2 uptake during the 2009/2010 El Niño event, presumably due to the insufficient spatial representativeness of the CO_2 and/or $\delta^{13}C$ data used in the analysis. It is also obvious that the oceanic CO_2 uptake increases with time, especially after 2000 when the fossil-fuel CO_2 emissions were rapidly increasing. Because anthropogenic CO_2 emitted into the atmosphere increases the CO_2 partial pressure difference between the atmosphere and ocean, it is expected that the oceanic CO_2 uptake has steadily increased. Previous studies reported that the oceanic CO_2 uptake has been increasing for the past several decades,[31] although the recent oceanic CO_2 uptake shown in Fig. 8 appears to be slightly larger than their estimates.

Keeling and Shertz[86] proposed the mass balance analysis of atmospheric CO_2 and O_2 for estimating the global carbon budget. The atmospheric O_2/N_2 ratio is currently decreasing with time in contrast to the CO_2 mole fraction, primarily due to fossil fuel consumption, and its trend is also related with the uptake or release of O_2 by the terrestrial biosphere. The terrestrial biospheric and oceanic CO_2 uptake values evaluated recently using this method are presented in Fig. 9.[85),87)–90)] The CO_2 uptake ranges between 1.0 and 1.6 GtC/yr for the terrestrial biosphere and between 2.2 and 2.6 GtC/yr for the ocean, with both showing a tendency to increase with time. This time-dependent increase is greater in case of the terrestrial biospheric uptake than in case of the oceanic uptake. Recently, Tohjima *et al.*[88] analyzed their 19-year

record of O_2/N_2 in the western Pacific and found that the 5-year average oceanic uptake monotonously increased with time in 2001–2014 and that the 5-year average terrestrial biospheric uptake showed a more complicated behavior, *i.e.*, a rapid increase in 2001–2009 and a rapid decrease in the subsequent period. As indicated in Fig. 3, the growth rate of atmospheric CO_2 exhibited almost no trend in the 2000s despite the continuously increasing fossil-fuel CO_2 emissions (see Fig. 8) during the period. The observation of Tohjima *et al.*[88] would lead to the possibility that anthropogenic CO_2 emitted into the atmosphere during this period was more efficiently absorbed by the terrestrial biosphere, which is inconsistent with the result shown in Fig. 8. To resolve this contradiction, it is required to observe $\delta^{13}C$ and O_2/N_2 over a wide geographical area and carefully assess the parameters used in the respective methods, *e.g.*, the isotopic disequilibrium flux in the $\delta^{13}C$ method and the oceanic O_2 outgassing in the O_2/N_2 method.

The estimations of the terrestrial biospheric and oceanic CO_2 fluxes using the atmospheric Bayesian inversion technique have also been actively performed. In this approach, *a priori* fluxes (or a set of guessed flux values) are optimized using global atmospheric transport models and atmospheric CO_2 observations, resulting in spatially distributed *posterior* flux values satisfying the uncertainties associated with *a priori* fluxes and observation data. The first extensive inversion project using three-dimensional atmospheric transport models was TransCom 3,[91] in which 16 different models participated to infer the CO_2 fluxes for 22 assigned regions of the world (11 for land and 11 for ocean) based on common CO_2 observation data and *a priori* CO_2 fluxes. Figure 10 shows the model average CO_2 fluxes over 1992–1996 for ten abbreviated areas. As shown in this figure, the *posterior* CO_2 fluxes are clearly different from the *a priori* fluxes, especially for the northern land and southern ocean regions, and the within-model uncertainties are smaller than the prescribed values, implying that the fluxes are well constrained by the atmospheric CO_2 observations. However, the fluxes estimated for the tropical land and southern land areas exhibit large uncertainties due to a limited number of CO_2 observations. The terrestrial biosphere serves as a source in the tropics and a sink in the northern area and is neutral in the southern area, and the ocean serves as a source in the tropics and a sink in the northern and southern areas.

The TransCom 3 estimated the global oceanic CO_2 uptake to be 1.3 (1.7–2.1), 0.8 (1.2–1.6), 1.4 (1.8–2.2), and 1.1 (1.5–1.9) GtC/yr for 1992–1996, 1980–1989, 1990–1999, and 1980–1999, respectively, and the corresponding terrestrial biospheric CO_2 uptake to be 1.3 (0.9–0.5), 1.5 (1.1–0.7), 1.7 (1.3–0.9), and 1.6 (1.2–0.8) GtC/yr. Because the atmospheric inversion method infers only the net flux between the atmosphere and terrestrial biosphere or ocean at a specified time, it is necessary to correct for the riverine transport of carbon from land to oceans. The above numbers in parentheses represent the results corrected by assuming the pre-industrial steady-state fluxes to be 0.4–0.8 GtC/yr.[30]

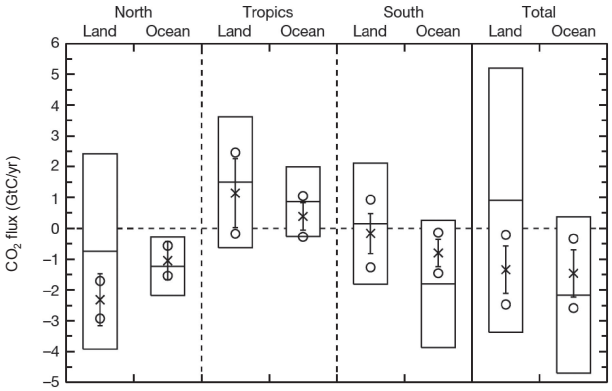

Fig. 10. Average terrestrial biospheric and oceanic CO_2 fluxes for global, northern, tropical, and southern areas over 1992–1996 derived from the TransCom 3 atmospheric inversions (Gurney *et al.*[91]). The boxes represent the *a priori* fluxes (center) and their uncertainties (upper and lower bounds), the crosses and vertical bars indicate the average *posterior* fluxes and one-standard deviations of the results from 16 models, respectively, and the circles denote the average uncertainties of the *posterior* fluxes.

After the TransCom 3 exercise, atmospheric inversions were conducted more extensively not only by enriching the surface data but also by including aircraft or satellite observations, revealing spatio-temporal varying fluxes and changes in the global carbon cycle due to human activities.[58),92)–100] As mentioned above, TransCom 3 found a large tropical land CO_2 source, but such a large source was later found to be in contradiction to the results obtained by Stephens *et al.*[101] Smaller or almost zero emissions were suggested by the recent atmospheric CO_2 inverse models with improved transport parameterization and a more advanced data assimilation framework.[100] Although atmospheric inversion assumes anthropogenic CO_2 emissions to be estimated with sufficient accuracy, their uncertainties have a non-negligible impact on the estimation of the terrestrial biospheric and oceanic fluxes.[100),102]

Table 1. Global budgets of anthropogenic CO_2 estimated by Le Quéré *et al.*[31] for six decadal periods from 1960 to 2017

	Mean (GtC/yr)					
	1960–1969	1970–1979	1980–1989	1990–1999	2000–2009	2008–2017
Total emissions ($E_{ff} + E_{luc}$)						
Fossil CO_2 emissions (E_{ff})	3.1 ± 0.2	4.7 ± 0.2	5.4 ± 0.3	6.3 ± 0.3	7.8 ± 0.4	9.4 ± 0.5
Land-use change emissions (E_{luc})	1.5 ± 0.7	1.2 ± 0.7	1.2 ± 0.7	1.4 ± 0.7	1.3 ± 0.7	1.5 ± 0.7
Total emissions	4.7 ± 0.7	5.8 ± 0.7	6.6 ± 0.8	7.6 ± 0.8	9.0 ± 0.8	10.8 ± 0.8
Partitioning						
Growth rate in atmospheric CO_2 conc. (G_{atm})	1.7 ± 0.07	2.8 ± 0.07	3.4 ± 0.02	3.1 ± 0.02	4.0 ± 0.02	4.7 ± 0.02
Ocean sink (S_{ocean})	1.0 ± 0.5	1.3 ± 0.5	1.7 ± 0.5	2.0 ± 0.5	2.1 ± 0.5	2.4 ± 0.5
Terrestrial sink (S_{land})	1.2 ± 0.5	2.1 ± 0.4	1.8 ± 0.6	2.4 ± 0.5	2.7 ± 0.7	3.2 ± 0.7
Budget imbalance						
$B_{im} = E_{ff} + E_{luc} - (G_{atm} + S_{ocean} + S_{land})$	0.6	−0.3	−0.3	0.2	0.2	0.5

More detailed global carbon budgets were examined by Le Quéré *et al.*[31] for 1960–2017 as part of the Global Carbon Project (https://www.globalcarbonproject.org/). In their study, five components, *i.e.*, the atmospheric CO_2 growth rate (G_{atm}), CO_2 emission from fossil fuel consumption/cement production (E_{ff}), CO_2 emission from land-use change (E_{luc}), oceanic CO_2 sink (S_{ocean}), and terrestrial biospheric CO_2 sink (S_{land}), were evaluated by primarily using the globally averaged surface CO_2 data obtained by the NOAA/ESRL/GMD, energy consumption data combined with emission factors/cement production data, bookkeeping models, global ocean biogeochemistry models and dynamic global vegetation models, respectively. They also inspected E_{luc} and S_{ocean} using the global vegetation models and ΔpCO_2 observations, respectively, and S_{ocean} and S_{land} using atmospheric inversions. It was found from their results that the CO_2 fluxes derived using different methods for each component were close on average to each other, but the respective fluxes had large uncertainties. Their results are summarized in Table 1. E_{ff} increases from 3.1 GtC/yr in 1960–1969 to 9.4 GtC/yr in 2008–2017, whereas E_{luc} is almost constant at 1.4 GtC/yr, indicating that the recent emissions of anthropogenic CO_2 are mainly caused by fossil fuel combustion. The growth rate of atmospheric CO_2 (G_{atm}) increases from 1.7 GtC/yr in 1960–1969 to 4.7 GtC/yr in 2008–2017. The terrestrial biospheric (S_{land}) and oceanic (S_{ocean}) sinks also intensify from 1.2 GtC/yr in 1960–1969 to 3.2 GtC/yr in 2008–2017 and from 1.0 to 2.4 GtC/yr in the corresponding periods, respectively. The global CO_2 emissions must be equal to their partitions among the atmosphere, terrestrial biosphere, and ocean, but there is a small imbalance between $E_{ff} + E_{luc}$ and $G_{atm} + S_{land} + S_{ocean}$. Because the uncertainties of G_{atm} and E_{ff} are small, the budget imbalance is primarily attributed to the model estimates of E_{luc}, S_{land}, and S_{ocean}.

The zonal mean CO_2 fluxes deduced by Le Quéré *et al.*[31] using the atmospheric inversions and process models show different temporal variations depending on the latitude zone. In the northern extratropics (north of 30°N), the atmosphere-to-land/ocean CO_2 fluxes gradually increase with time, but the ensemble-mean total fluxes of the process models are lower than the estimates obtained using the inversions, mainly due to the difference in land flux between the two approaches. In the tropics (30°N–30°S), both the process models and inversions indicate that the carbon balance is almost neutral on average for land and ocean, with large year-to-year variability of land flux. In the southern extratropics (south of 30°S), the oceanic CO_2 sink is gradually enhanced with time, while the land source and sink are almost balanced, and the oceanic uptake inferred from the atmospheric inversions is slightly higher than that obtained from the process models.

Le Quéré *et al.*[31] reported the global anthropogenic carbon budget for 1750–2017. The five component values before 1960 were estimated using the energy consumption/cement production data for fossil-fuel CO_2 emissions, the bookkeeping models for land-use change CO_2 emissions, the ice core data for the growth rate of atmospheric CO_2, the diagnostic ocean models for the oceanic CO_2 uptake, and the

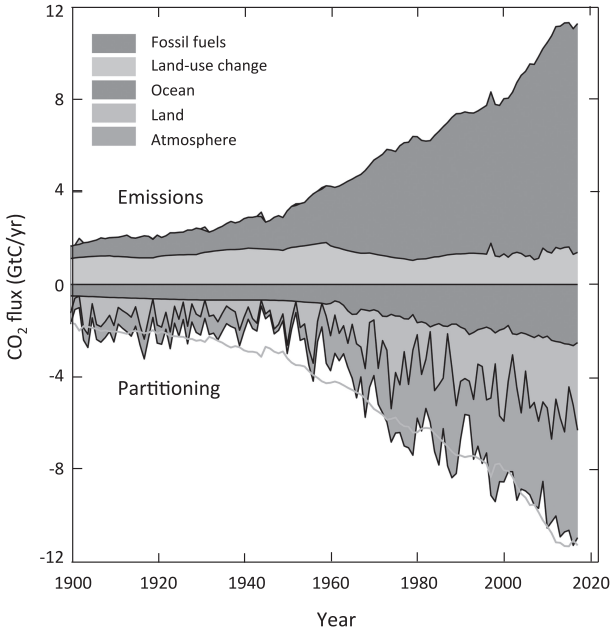

Fig. 11. Global carbon budget based on two emissions of fossil fuels and land-use change and three sinks of oceanic uptake, terrestrial biospheric uptake, and atmospheric residue (from top to bottom in the figure) for 1900–2017 (Le Quéré *et al.*[31]). The gray line in the lower panel represents the total emissions, the sign of which is reversed.

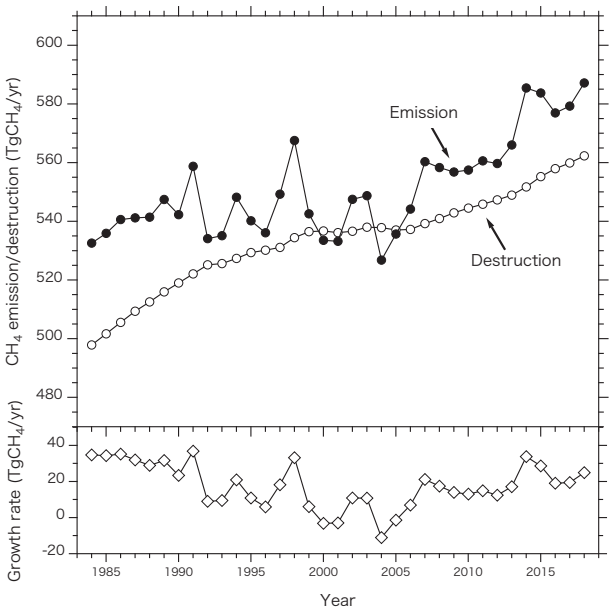

Fig. 12. Global CH_4 emission and destruction (upper panel) calculated for each year from 1984 to 2018 and the corresponding growth rate of atmospheric CH_4 (lower panel).

global vegetation models for the terrestrial biospheric CO_2 uptake. The results obtained are presented in Fig. 11. The fossil-fuel CO_2 emissions increased gradually before and rapidly after the Second World War, and the terrestrial biospheric CO_2 emissions gradually increased until around 1960 and then gradually decreased toward an almost constant value after 1980. The cumulative CO_2 emissions for 1750–2017 are 430 ± 20 GtC for E_{ff} and 235 ± 95 GtC for E_{luc}, showing a large uncertainty for E_{luc}. The anthropogenic CO_2 is partitioned among the atmosphere (275 ± 5 GtC), terrestrial biosphere (215 ± 50 GtC), and ocean (165 ± 20 GtC), with large uncertainties for the terrestrial and oceanic CO_2 uptake. Thus, the cumulative budget imbalance is 10 GtC. If the period is limited to 1850–2017, the budget imbalance increases to 25 GtC. This imbalance is probably due to the overestimation of E_{luc} and/or underestimation of the terrestrial and oceanic CO_2 uptake from the mid-1920s to the mid-1960s because atmospheric CO_2 shows no appreciable increase during this period.

4.2. Methane. By assuming the atmosphere to be one well-mixed box, the global mass balance of atmospheric CH_4 can be expressed as

$$m_{CH_4} n_{air} \frac{dC_{CH_4}}{dt} = S_{CH_4} - m_{CH_4} n_{air} \frac{C_{CH_4}}{\tau_{CH_4}}, \quad [2]$$

where m_{CH_4} is the average molecular weight of CH_4, n_{air} is the number of moles of the atmosphere, C_{CH_4} is the atmospheric CH_4 mole fraction, S_{CH_4} is the CH_4 emission, and τ_{CH_4} is the lifetime of CH_4 in the atmosphere. Figure 12 shows the global CH_4 emission and destruction calculated for each year from 1984 to 2018 using the NOAA/ESRL/GMD global average CH_4 data and the corresponding growth rate of atmospheric CH_4 constrained by adopting an atmospheric CH_4 lifetime of 9.1 years.[34] As mentioned before, the CH_4 growth rate gradually declined from around 1990 to the mid-2000s, which means that the global CH_4 budget approached a steady state with no CH_4 emission trend. The calculated CH_4 emissions were almost constant at 542 $TgCH_4$/yr for 1984–2005, and then increased with time until it became 587 $TgCH_4$/yr in 2018. On the other hand, the CH_4 destruction increased gradually from 498 $TgCH_4$/yr in 1984 to 562 $TgCH_4$/yr in 2018, and both the CH_4 emission and destruction were 537 $TgCH_4$/yr in 2000–2005 when the atmospheric CH_4 increase stagnated.

Kirschke *et al.*[32] evaluated the atmospheric CH_4 lifetime to be 8–10 years by inspecting the results of earlier studies in terms of uncertainty and

variability. If 8 and 10 years are employed as the lifetimes, the average CH_4 emissions for 1984–2005 are 614 and 495 $TgCH_4$/yr, respectively, with the difference between the two values being as much as 119 $TgCH_4$/yr. This implies that an accurate determination of the CH_4 lifetime, *i.e.*, of the atmospheric OH concentration, is extremely crucial to understand the global CH_4 budget.

The Global Carbon Project has published two papers to depict a current picture of the global CH_4 budget based on the knowledge obtained using the bottom-up and top-down approaches.[32),33)] In this paper, we mainly discuss the results reported by Saunois *et al.*[33)] for 2003–2012 by citing Kirschke *et al.*[32)] when necessary. The average global CH_4 budget obtained by Saunois *et al.*[33)] for 2003–2012 are presented in Table 2 along with that obtained by Kirschke *et al.*[32)] for 2000–2009. As can be understood from the maximum and minimum estimates in brackets, there is a considerable amount of uncertainty associated with the mean value reported for each sector. Based on the inventories for fossil fuels, agriculture, wastes, and biomass and biofuel burning, Saunois *et al.*[33)] estimated the mean anthropogenic CH_4 emissions to be 352 $TgCH_4$/yr for 2003–2012 and 338 $TgCH_4$/yr for 2000–2009 (not shown in the table). The latter value is consistent with the value of 331 $TgCH_4$/yr reported by Kirschke *et al.*[32)] for the same period using the same approach. The "agriculture and waste" sector constitutes the largest anthropogenic emission of CH_4, followed by "fossil fuels", with "biomass and biofuel burning" as the lowest contributor. On the other hand, natural CH_4 emissions are clearly different between the two studies. Saunois *et al.*[33)] estimated the mean natural emissions to be 384 $TgCH_4$/yr for 2003–2012 and 382 $TgCH_4$/yr for 2000–2009, showing very little change in the emission between these two periods. However, their estimates are 10% larger than the value obtained by Kirschke *et al.*[32)] for 2000–2009. A large discrepancy between the two studies is found in case of "other natural sources", resulting from "fresh waters" being grouped into "other land sources", probably due to the use of different land surface models as well as the prescribed difference in the size of the wetland extent between the two studies. A large discrepancy is also found in "natural wetlands". The CH_4 emissions estimated by Saunois *et al.*[33)] for 2003–2012 and 2000–2009 are in good agreement with each other, but their estimates are 15% smaller than the value of Kirschke *et al.*[32)] for 2000–2009. With respect to the CH_4 sinks, Saunois *et al.*[33)] adopted a climatological range, similar to Kirschke *et al.*[32)] for 2000–2009. As shown in the table, tropospheric Cl destroys only a small amount of CH_4, but it is known that this element considerably affects the interpretation of the observed $\delta^{13}C$ of atmospheric CH_4 due to the large kinetic isotope effect in the reaction with CH_4.[103)]

The top-down estimates by Saunois *et al.*[33)] for individual sources were obtained as ensemble averages of multi-atmospheric inversions, wherein the atmospheric lifetime of CH_4 was reasonably assumed. The total global CH_4 emission was 558 $TgCH_4$/yr for 2003–2012 and 552 $TgCH_4$/yr for 2000–2009. The latter value is very close to the value of 553 $TgCH_4$/yr given by Kirschke *et al.*[32)] for the same period, indicating the effectiveness of the flux constraint based on atmospheric observations. However, these top-down estimates are considerably smaller than the high bottom-up value of 736 $TgCH_4$/yr that can be primarily attributed to overestimation by the bottom-up method with no constraint based on atmospheric CH_4 measurements. Among the total global CH_4 emission for 2003–2012, 60% was allocated to anthropogenic sources, and the remaining 40% was allocated to natural sources. The atmospheric inversion results of 188, 105, and 34 $TgCH_4$/yr for "agriculture and waste", "fossil fuels", and "biomass and biofuel burning", respectively, are statistically consistent with the values obtained using the bottom-up approach. On the other hand, the CH_4 emissions from natural sources are considerably different between the two approaches, and the top-down estimate of 231 $TgCH_4$/yr is 60% of the bottom-up value of 384 $TgCH_4$/yr, mainly due to a big discrepancy in the estimates for "other natural sources". Similar agreement and disagreement between the two approaches are found in Kirschke *et al.*[32)]

Saunois *et al.*[33)] found that in 2003–2012, 64%, 32%, and 4% of the total global CH_4 emissions originated from the tropics and southern latitudes (<30°N), the northern mid-latitudes (30°–60°N), and the northern high latitudes (>60°N), respectively. Majority of the emissions originated from Africa, South America, and South East Asia (73–86 $TgCH_4$/yr), constituting about 44% of the total global emissions. These high-emission regions were then followed by China, central Eurasia and Japan, contiguous U.S.A., Russia, India, and Europe (28–58 $TgCH_4$/yr). The remaining regions emit 7–20 $TgCH_4$/yr of CH_4. Saunois *et al.*[33)] reported that different CH_4 budget estimates were obtained by

Table 2. Global budgets of CH_4 ($TgCH_4$/yr) estimated by Saunois *et al.*[33] for 2003–2012 and Kirschke *et al.*[32] for 2000–2009 using the bottom-up and top-down approaches

	Saunois *et al.* (2016) Bottom-up	Saunois *et al.* (2016) Top-down	Kirschke *et al.* (2013) Bottom-up	Kirschke *et al.* (2013) Top-down
Period of time	2003–2012	2003–2012	2000–2009	2000–2009
Natural sources	384 [257–524]	231 [194–296]	347 [238–484]	218 [179–273]
Natural wetlands	185 [153–227]	167 [127–202]	217 [177–284]	175 [142–208]
Other natural sources	199 [104–297]	64 [21–132]	130 [45–232]	43 [37–65]
Other land sources	185 [99–272]		112 [43–192]	
Fresh waters	122 [60–180]		40 [8–73]	
Geological (onshore)	40 [30–56]		36 [15–57]	
Wild animals	10 [5–15]		15 [15–15]	
Termites	9 [3–15]		11 [2–22]	
Wildfires	3 [1–5]		3 [1–5]	
Permafrost soils	1 [0–1]		1 [0–1]	
Vegetation				
Ocean sources	14 [5–25]		18 [2–40]	
Geological (offshore)	12 [5–20]			
Other (including hydrates)	2 [0–5]			
Anthropogenic sources	352 [340–360]	328 [259–370]	331 [304–368]	335 [273–409]
Agriculture and waste	195 [178–206]	188 [115–243]	200 [187–224]	209 [180–241]
Enteric fermentation & manure	106 [97–111]		101 [98–105]	
Landfills & waste	59 [52–63]		63 [56–79]	
Rice cultivation	30 [24–36]		36 [33–40]	
Fossil fuels	121 [114–133]	105 [77–133]	96 [85–105]	96 [77–123]
Coal mining	41 [26–50]			
Gas, oil & industry	79 [69–88]			
Biomass & biofuel burning	30 [27–35]	34 [15–53]	35 [32–39]	30 [24–45]
Biomass burning	18 [15–21]			
Biofuel burning	12 [10–14]			
Sinks				
Total chemical loss		515	604 [483–738]	518 [510–538]
Tropospheric OH			528 [454–617]	
Stratospheric loss			51 [16–84]	
Tropospheric Cl			25 [13–37]	
Soil uptake		33 [28–38]	28 [9–47]	32 [26–42]
Sum of sources	736 [596–884]	558 [540–568]	678 [542–852]	553 [526–569]
Sum of sinks		548	632 [592–785]	550 [514–560]
Imbalance		10		3 [−4–19]
Atmospheric growth		10.0 [9.4–10.6]		6

replacing ground-based observations with satellite-based observations, especially in the tropical region in which surface observations were sparse. This attests to the fact that an extensive observational spatial coverage is crucial for obtaining realistic CH_4 fluxes using the inversion approach.

4.3. Nitrous oxide. To estimate the global N_2O budget over the last 40 years, the one-box mass balance equation, *i.e.*,

$$m_{N_2O} n_{air} \frac{dC_{N_2O}}{dt} = S_{N_2O} - m_{N_2O} n_{air} \frac{C_{N_2O}}{\tau_{N_2O}}, \quad [3]$$

is applied to the N_2O data shown in Fig. 7. Here, the respective variables have almost the same meaning as the variables in Eq. [2]. The atmospheric lifetime is an essential factor for evaluating the N_2O budget. Previous lifetime estimates range from 114 to 131 years, with an associated uncertainty of 10 to 30 years.[34),36),39)] Here, we employ 120 years as the N_2O lifetime, which is widely used in other studies. The results obtained for 1979–2017 show that the atmospheric burden is 1513.7 TgN, the destruction is 12.6 TgN/yr, the atmospheric growth is 3.8 TgN/yr, and the emission is 16.4 TgN/yr. Based on the assumption that the atmospheric mole fraction and lifetime of N_2O in the pre-industrial era were 270 ppb and 120 years, respectively, N_2O emitted naturally from soils and oceans was calculated to be 10.8 TgN/yr, yielding an anthropogenic N_2O emission of 5.6 TgN/yr for 1979–2017. With regard to the N_2O lifetime, Prather *et al.*[34)] reported the current and pre-industrial (around 1750) values to be 131 and 142 years, respectively. If these lifetime values are used, the N_2O destruction and emission for 1979–2017 decrease to 11.6 and 15.4 TgN/yr, respectively, and the natural N_2O emission also decreases to 9.1 TgN/yr. Further, the anthropogenic N_2O emission increases to 6.3 TgN/yr.

The atmospheric inversion technique was first applied by Hirsch *et al.*[104)] and then by Huang *et al.*,[105)] Saikawa *et al.*,[106)] and Thompson *et al.*[82)] In addition to these studies, TransCom N_2O intercomparison[107)] and the analysis proposed by Thompson *et al.*[108)] were also conducted using different atmospheric inversion frameworks. The global, land, and ocean N_2O fluxes obtained from these atmospheric inversions are shown in Fig. 13 along with the results of the aforementioned one-box model analysis with a lifetime of 120 years. The results obtained from different studies are generally consistent with each other within estimated uncertainties, except for the global N_2O fluxes derived by Thompson *et al.*[82)] and by one of the participants in TransCom N_2O, the values of which are appreciably higher than others. The results of Thompson *et al.*[108)] and the one-box model analysis indicate that global N_2O emissions increased steadily with time. It is also shown in this figure that the N_2O emissions from land are clearly higher than those from the ocean. The results of Hirsch *et al.*[104)] and Huang *et al.*[105)] allocated 2%, 28%, 50%, and 20% of the total global N_2O emissions to 90°–30°S, 30°S–0°, 0°–30°N, and 30°–90°N, respectively, and 7%, 28%, 41%, and 23% were estimated for the corresponding latitude bands

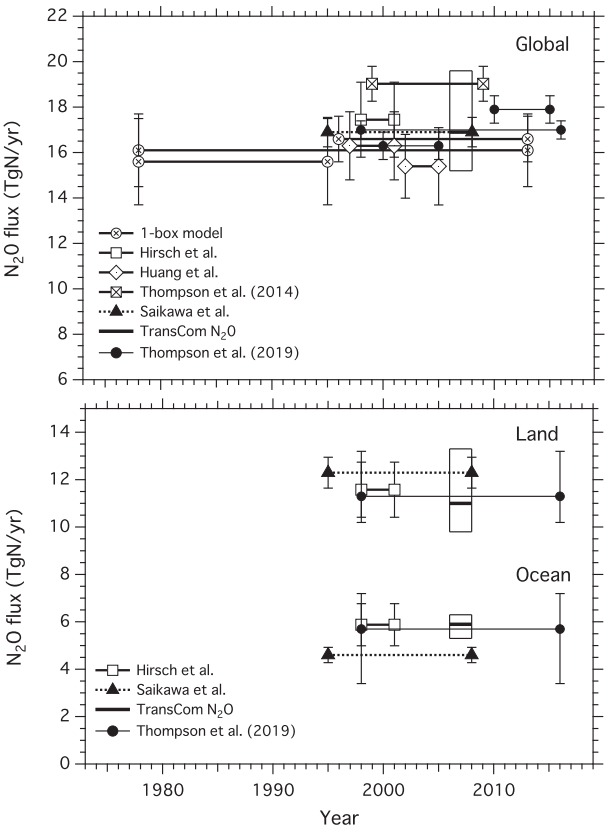

Fig. 13. Global, land, and ocean N_2O fluxes inferred from atmospheric inversions. The global flux obtained using the one-box mass balance analysis (*cf.* text) is also shown in the upper panel.

by the TransCom N_2O intercomparison exercise. These values indicate that the northern tropics and subtropics are most important for N_2O emissions, as suggested by the observed latitudinal distribution of atmospheric N_2O. The results of the atmospheric inversions show high N_2O emissions in East and South Asia, North, South, and Central America, and Africa on land and in the tropical (30°S–30°N) ocean.

The global N_2O budget was quantified using the bottom-up methods.[39),109)–111)] For example, on the basis of the existing bottom-up estimates, Ciais *et al.*[39)] reported global N_2O budgets for 2006 and the mid-1990s, as shown in Table 3. The 2006 budget indicates that agricultural activities are the strongest anthropogenic sources. The total N_2O emissions from "rivers", "estuaries", "coastal zone", and "atmospheric deposition on land and ocean" associated with anthropogenic reactive nitrogen species are also high (1.2 TgN/yr in total), followed by "fossil fuel combustion and industrial processes",

Table 3. Global budgets of N_2O (TgN/yr) estimated by Ciais *et al.*[39] for 2006 and the mid-1990s

	2006	mid-1990s
Anthropogenic sources		
Fossil fuel combustion & industrial processes	0.7 (0.2–1.8)	0.7 (0.2–1.8)
Agriculture	4.1 (1.7–4.8)	3.7 (1.7–4.8)
Biomass & biofuel burning	0.7 (0.2–1.0)	0.7 (0.2–1.0)
Human excreta	0.2 (0.1–0.3)	0.2 (0.1–0.3)
Rivers, estuaries, coastal zones	0.6 (0.1–2.9)	0.6 (0.1–2.9)
Atmospheric deposition on land	0.4 (0.3–0.9)	0.4 (0.3–0.9)
Atmospheric deposition on ocean	0.2 (0.1–0.4)	0.2 (0.1–0.4)
Total anthropogenic sources	6.9 (2.7–11.1)	6.5 (2.7–11.1)
Natural sources		
Soils under natural vegetation	6.6 (3.3–9.0)	6.6 (3.3–9.0)
Oceans	3.8 (1.8–9.4)	3.8 (1.8–9.4)
Atmospheric chemistry	0.6 (0.3–1.2)	0.6 (0.3–1.2)
Surface sink	−0.01 (0−−1.0)	−0.01 (0−−1.0)
Total natural sources	11.0 (5.5–19.6)	11.0 (5.4–19.6)
Total natural + anthropogenic sources	17.9 (8.1–30.7)	17.5 (8.1–30.7)
Stratospheric sink	14.3 (4.3–27.2)	
Observed growth rate	3.6 (3.5–3.8)	

"biomass and biofuel burning", and "human excreta". The N_2O emissions from agriculture increase from 3.7 TgN/yr in the mid-1990s to 4.1 TgN/yr in 2006, resulting in an increase of 6% with respect to the total global anthropogenic emissions. On the other hand, the natural N_2O emissions from "soils under natural vegetation", "oceans", and "atmospheric chemistry" (mainly by NH_3 oxidation) contribute 60%, 35%, and 5%, respectively, to the global total. The surface sink of N_2O is also presented in the table, but its strength is negligibly small. The stratospheric N_2O loss is usually inferred using atmospheric chemistry models,[35] but a value of 14.3 TgN/yr for "stratospheric sink" in Table 3 was derived by adjusting the model-calculated sinks to become equal to the difference between the total emission and the observed growth rate. If we use this value for the stratospheric sink, then the lifetime of N_2O is estimated to be 107 years because the atmospheric N_2O burden was 1535 TgN in 2006. This lifetime is slightly shorter than the aforementioned lifetime of 114–131 years. It is likely that the natural and/or anthropogenic N_2O emissions are overestimated. Table 3 shows that 6.5–6.9 TgN/yr of N_2O has been recently emitted into the atmosphere due to human activities and that 11.0 TgN/yr of N_2O has been emitted due to natural causes, with the total being 17.5–17.9 TgN/yr. These values are at the upper end of the results deduced from the above-mentioned mass balance analyses and atmospheric inversions. The individual estimates are still rather scattered, and their uncertainties are considerably large. Further studies are required to more accurately infer the global N_2O budget.

5. Concluding remarks

The observation of anthropogenic changes in atmospheric greenhouse gases serves as an indicator of the progress of human-induced climate change and is necessary for elucidating their global cycling. Such scientific knowledge forms the basis for formulating and implementing strategies to mitigate the radiatively forced climate change.

The present global network of greenhouse gas observations consists mainly of 100–150 ground-based sites. However, these sites are unevenly distributed in space, with a very limited number of observations in the tropics, such as Africa, South America, and continental interiors. To obtain a detailed picture of the variability of atmospheric greenhouse gases (mole fractions, isotope ratios, and other relevant elements) in space and time, it is important to not only fill in the geographically blank areas in the observation network with additional stations but also perform measurements using aircraft, balloons, and satellites. Because the satellite observations retrieve related variables from spectral radiance, careful validation of the results is indispensable for use along with direct and calibrated measurements. The data thus obtained will contribute to constraining the global budget estimations of anthropogenic greenhouse gases more robustly. They are also useful for developing and validating various types of models, including atmospheric chemistry/transport models, global ocean biogeochemistry models, and dynamic global vegetation models.

It is also important to know the temporal variations of atmospheric greenhouse gases before conducting modern systematic observations. The analysis of the air occluded in the polar ice cores was one of the most promising methods for this

purpose. For example, deep Antarctic ice cores revealed that atmospheric CO_2, CH_4, and N_2O fluctuated considerably over the last 800 kyrs, showing interglacial–glacial and interstadial–stadial cycles. The low mole fraction values observed in the glacial periods have been interpreted as an enhancement in the oceanic uptake of CO_2 and a reduction in the emissions for CH_4 and N_2O, but their detailed processes and impact on global climate change are not yet fully understood. The high-resolution variations in atmospheric greenhouse gases over the past 2000 years have also been reconstructed from the air bubbles in polar ice cores drilled at locations with high snow accumulation rates, as well as from the firn air collected from the surface layer of the ice sheet. These data, which include isotope ratios, have been used to estimate the time-dependent emissions and sinks of greenhouse gases. However, to obtain more robust and quantitative knowledge on the global cycling of natural and anthropogenic greenhouse gases and their impact on climate, further detailed analyses using mole fraction and isotope data, climate proxies, and models are required.

Top-down and bottom-up approaches have been adopted to quantify the global budgets of anthropogenic greenhouse gases. In the top-down approach, emission balances the sum of sink and atmospheric growth, but the individual source and sink components are not quantified well. To employ this approach more effectively, it is necessary to reasonably estimate the lifetime of atmospheric greenhouse gases, collect atmospheric observation data from a close-configured station network, and develop well-validated atmospheric chemistry/transport models. For atmospheric inverse modeling, *a priori* fluxes and uncertainties must be realistically prescribed because *posterior* fluxes are sensitive to them. In the bottom-up approach, the fluxes of individual sources or sinks can be assessed independently, but their uncertainties are usually quite large, with the exception of fossil-fuel CO_2 emissions, and large budget imbalances are often found in the results. Moreover, previous studies have often indicated that source and sink estimates obtained even in a similar way are different depending on individual studies. Thus, it is necessary that the respective approaches are improved and complement each other to achieve accurate budget assessments.

Further studies are needed to understand the response of global and regional source and sink fluxes to future climate change using global biogeochemical models coupled with climate models. To verify the results obtained from such studies, the naturally caused variations in the mole fraction, isotope ratios and other relevant components observed in the atmosphere or reconstructed from the polar ice cores and firn air would be helpful.

Acknowledgements

The author expresses his sincere thanks to Dr. R. F. Keeling (Scripps Institution of Oceanography), Dr. E. J. Dlugokencky (NOAA/ESRL/GMD), Dr. R. G. Prinn (Massachusetts Institute of Technology), and Dr. R. F. Weiss (Scripps Institution of Oceanography) for providing their updated mole fraction data for this paper, and to Ms. A. Okamoto and Dr. S. Nakaoka (National Institutes for Environmental Studies) for their help in preparing Fig. 1.

References

1) Petit, J.R., Jouzel, J., Raynaud, D., Barkov, N.I., Barnola, J.M., Basile, I. *et al.* (1999) Climate and atmospheric history of the past 420,000 years from the Vostok ice core, Antarctica. Nature **399**, 429–436.
2) Kawamura, K., Parrenin, F., Lisiecki, L., Uemura, R., Vimeux, F., Severinghaus, J.P. *et al.* (2007) Northern Hemisphere forcing of climatic cycles in Antarctica over the past 360,000 years. Nature **448**, 912–916.
3) Schilt, A., Baumgartner, M., Blunier, T., Schwander, J., Spahni, R., Fischer, H. *et al.* (2010) Glacial–interglacial and millennial-scale variations in the atmospheric nitrous oxide concentration during the last 800,000 years. Quat. Sci. Rev. **29**, 182–192.
4) Keeling, C.D., Adams, J.A.J., Ekdahl, C.A.J. and Guenther, P.R. (1976) Atmospheric carbon dioxide variations at the South Pole. Tellus **28**, 552–564.
5) Keeling, C.D., Bacastow, R.B., Bainbridge, A.E., Ekdahl, C.A.J., Guenther, P.R. and Waterman, L.S. (1976) Atmospheric carbon dioxide variations at Mauna Loa Observatory, Hawaii. Tellus **28**, 538–551.
6) Dlugokencky, E.J., Steele, L.P., Lang, P.M. and Masarie, K.A. (1994) The growth rate and distribution of atmospheric methane. J. Geophys. Res. **99**, 17021–17043.
7) Machida, T., Nakazawa, T., Fujii, Y., Aoki, S. and Watanabe, O. (1995) Increase in the atmospheric nitrous oxide concentration during the last 250 years. Geophys. Res. Lett. **22**, 2921–2924.
8) Prinn, R.G., Weiss, R.F., Arduini, J., Arnold, T., DeWitt, H.L., Fraser, P.J. *et al.* (2018) History of chemically and radiatively important atmospheric gases from the Advanced Global Atmospheric Gases Experiment (AGAGE). Earth Syst. Sci. Data **10**, 985–1018.
9) Rubino, M., Etheridge, D.M., Thornton, D.P.,

Howden, R., Allison, C.E., Francey, R.J. *et al.* (2019) Revised records of CO_2, CH_4, N_2O, and δ^{13}C-CO_2 from Law Dome, Antarctica. Earth Syst. Sci. Data **11**, 473–492.
10) IPCC (2013) Summary for policymakers. *In* Climate Change 2013: The Physical Science Basis. Contribution of Working Group I to the Fifth Assessment Report of the Intergovernmental Panel on Climate Change (eds. Stocker, T.F., Qin, D., Plattner, G.-K., Tignor, M., Allen, S.K., Boschung, J. *et al.*). Cambridge University Press, Cambridge, United Kingdom and New York, U.S.A., pp. 3–29.
11) Callendar, G.S. (1938) The artificial production of carbon dioxide and its influence on temperature. Q. J. R. Meteorol. Soc. **64**, 223–237.
12) Fraser, P.J., Khalil, M.A.K., Rasmussen, R.A. and Crawford, A.J. (1981) Trends of atmospheric methane in the Southern Hemisphere. Geophys. Res. Lett. **8**, 1063–1066.
13) Blake, D.R. and Rowland, F.S. (1986) World-wide increase in tropospheric methane, 1978–1983. J. Atmos. Chem. **4**, 43–62.
14) Weiss, R.F. (1981) The temporal and spatial distribution of tropospheric nitrous oxide. J. Geophys. Res. **86**, 7185–7195.
15) Elkins, J.W., Thompson, T.M., Swanson, T.H., Butler, J.H., Hall, B.D., Cummings, S.O. *et al.* (1993) Decrease in the growth rates of atmospheric chlorofluorocarbons 11 and 12. Nature **364**, 780–783.
16) Nakazawa, T., Morimoto, S., Aoki, S. and Tanaka, T. (1993) Time and space variations of the carbon isotopic ratio of tropospheric carbon dioxide over Japan. Tellus B **45**, 258–274.
17) Nakazawa, T., Morimoto, S., Aoki, S. and Tanaka, M. (1997) Temporal and spatial variations of the carbon isotopic ratio of atmospheric carbon dioxide in the western Pacific region. J. Geophys. Res. **102**, 1271–1285.
18) Nakazawa, T., Aoki, S., Kawamura, K., Saeki, T., Sugawara, S., Honda, H. *et al.* (2002) Variations of stratospheric trace gases measured using a balloon-borne cryogenic sampler. Adv. Space Res. **30**, 1349–1357.
19) Machida, T., Matsueda, H., Sawa, Y., Nakagawa, Y., Hirotani, H., Kondo, N. *et al.* (2008) Worldwide measurements of atmospheric CO_2 and other trace gas species using commercial airlines. J. Atmos. Ocean. Technol. **25**, 1744–1754.
20) Ishijima, K., Nakazawa, T. and Aoki, S. (2009) Variations of atmospheric nitrous oxide concentration in the northern and western Pacific. Tellus B **61**, 408–415.
21) Yokota, T., Yoshida, Y., Eguchi, N., Ota, Y., Tanaka, T., Watanabe, H. *et al.* (2009) Global concentrations of CO_2 and CH_4 retrieved from GOSAT: First preliminary results. Sci. Online Lett. Atmos. **5**, 160–163.
22) Eldering, A., O'Dell, C.W., Wennberg, P.O., Crisp, D., Gunson, M.R., Viatte, C. *et al.* (2017) The Orbiting Carbon Observatory-2: First 18 months of science data products. Atmos. Meas. Tech. **10**, 549–563.
23) Neftel, A., Oeschger, H., Schwander, J., Stauffer, B. and Zumbrunn, R. (1982) Ice core sample measurements give atmospheric CO_2 content during the past 40,000 yr. Nature **295**, 220–223.
24) Revell, R. and Suess, H.E. (1957) Carbon dioxide exchange between atmosphere and ocean and the question of an increase of atmospheric CO_2 during the past decades. Tellus **9**, 18–27.
25) Keeling, C.D., Piper, S.C. and Heimann, M. (1989) A three dimensional model of atmospheric CO_2 transport based on observed winds: 4. Mean annual gradients and interannual variations. *In* Aspects of Climate Variability in the Pacific and the Western Americas (ed. Peterson, D.H.). American Geophysical Union, Washington, D.C., pp. 305–363.
26) Tans, P.P., Conway, T.J. and Nakazawa, T. (1989) Latitudinal distribution of the sources and sinks of atmospheric carbon dioxide from surface observations and an atmospheric transport model. J. Geophys. Res. **94**, 5151–5172.
27) Ehhalt, D.H. (1974) Atmospheric cycle of methane. Tellus **26**, 58–70.
28) Fung, I., John, J., Lerner, J., Matthews, E., Prather, M., Steele, L.P. *et al.* (1991) Three-dimensional model synthesis of the global methane cycle. J. Geophys. Res. **96**, 13033–13065.
29) Bouwman, A.F. and Taylor, J.A. (1996) Testing high-resolution nitrous oxide emission estimates against observations using an atmospheric transport model. Global Biogeochem. Cycles **10**, 307–318.
30) Resplandy, L., Keeling, R.F., Rodenbeck, C., Stephens, B.B., Khatiwala, S., Rodgers, K.B. *et al.* (2018) Revision of global carbon fluxes based on a reassessment of oceanic and riverine carbon transport. Nat. Geosci. **11**, 504–509.
31) Le Quéré, C., Andrew, R.M., Friedlingstein, P., Sitch, S., Hauck, J., Pongratz, J. *et al.* (2018) Global carbon budget 2018. Earth Syst. Sci. Data **10**, 1–54.
32) Kirschke, S., Bousquet, P., Ciais, P., Saunois, M., Canadell, J.G., Dlugokencky, E.J. *et al.* (2013) Three decades of global methane sources and sinks. Nat. Geosci. **6**, 813–823.
33) Saunois, M., Bousquet, P., Poulter, B., Peregon, A., Ciais, P., Canadell, J.G. *et al.* (2016) The global methane budget 2000–2012. Earth Syst. Sci. Data **8**, 697–751.
34) Prather, M.J., Holmes, C.D. and Hsu, J. (2012) Reactive greenhouse gas scenarios: Systematic exploration of uncertainties and the role of atmospheric chemistry. Geophys. Res. Lett. **39**, L09803.
35) Minschwaner, K., Salawitch, R.J. and McElroy, M.B. (1993) Absorption of solar radiation by O_2: Implications for O_3 and lifetimes of N_2O, $CFCl_3$ and CF_2Cl_2. J. Geophys. Res. **98**, 10543–10561.
36) Volk, C.M., Elkins, J.W., Fahey, D.W., Dutton,

G.S., Gilligan, J.M., Loewenstein, M. *et al.* (1997) Evaluation of source gas lifetimes from stratospheric observations. J. Geophys. Res. **102**, 25543–25564.

37) Kaiser, J., Rockmann, T., Brenninkmeijer, C.A.M. and Crutzen, P.J. (2003) Wavelength dependence of isotope fractionation in N_2O photolysis. Atmos. Chem. Phys. **3**, 303–313.

38) Wrage, N., Velthof, G.L., van Beusichem, M.L. and Oenema, O. (2001) Role of nitrifier denitrification in the production of nitrous oxide. Soil Biol. Biochem. **33**, 1723–1732.

39) Ciais, P., Sabine, C., Bala, G., Bopp, L., Brovkin, V., Canadell, J. *et al.* (2013) Carbon and other biogeochemical cycles. *In* Climate Change 2013: The Physical Science Basis. Contribution of Working Group I to the Fifth Assessment Report of the Intergovernmental Panel on Climate Change (eds. Stocker, T.F., Qin, D., Plattner, G.-K., Tignor, M., Allen, S.K., Boschung, J. *et al.*). Cambridge University Press, Cambridge, United Kingdom and New York, NY, U.S.A., pp. 465–570.

40) Curry, W.B., Duplessy, J.C., Labeyrie, L.D. and Shackleton, N.J. (1988) Changes in the distribution of $\delta^{13}C$ of deep water ΣCO_2 between the last glaciation and the Holocene. Paleoceanography **3**, 317–341.

41) Broecker, W.S. (1982) Ocean chemistry during glacial time. Geochim. Cosmochim. Acta **46**, 1689–1705.

42) Sigman, D.M. and Boyle, E.A. (2000) Glacial/interglacial variations in atmospheric carbon dioxide. Nature **407**, 859–869.

43) Kohfeld, K.E. and Ridgwell, A. (2009) Glacial-interglacial variability in atmospheric CO_2. *In* Surface Ocean-Lower Atmosphere Processes (eds. Le Quéré, C. and Saltzman, E.S.). American Geophysical Union, Washington, D.C., pp. 251–286.

44) Sigman, D.M., Hain, H.P. and Haug, G.H. (2010) The polar ocean and glacial cycles in atmospheric CO_2 concentration. Nature **466**, 47–55.

45) Martin, J.H. (1990) Glacial-interglacial CO_2 change: The iron hypothesis. Paleoceanography **5**, 1–13.

46) Stephens, B.B. and Keeling, R.F. (2000) The influence of Antarctic sea ice on glacial-interglacial CO_2 variations. Nature **404**, 171–174.

47) Archer, D.E., Martin, P.A., Milovich, J., Brovkin, V., Plattner, G.-K. and Ashendel, C. (2003) Model sensitivity in the effect of Antarctic sea ice and stratification on atmospheric pCO_2. Paleoceanography **18**, 1012.

48) Levine, J.G., Wolff, E.W., Jones, A.E., Sime, L.C., Valdes, P.J., Archibald, A.T. *et al.* (2011) Reconciling the changes in atmospheric methane sources and sinks between the Last Glacial Maximum and the pre-industrial era. Geophys. Res. Lett. **38**, L23804.

49) Murray, L.T., Mickley, L.J., Kaplan, J.O., Sofen, E.D., Pfeiffer, M. and Alexander, B. (2014) Factors controlling variability in the oxidative capacity of the troposphere since the Last Glacial Maximum. Atmos. Chem. Phys. **14**, 3589–3622.

50) Chappellaz, J.A., Fung, I.Y. and Thompson, A.M. (1993) The atmospheric CH_4 increase since the Last Glacial Maximum; (1) source estimates. Tellus B **45**, 228–241.

51) Weber, S.L., Drury, A.J., Toonen, W.H.J. and van Weele, M. (2010) Wetland methane emissions during the Last Glacial Maximum estimated from PMIP2 simulations: Climate, vegetation, and geographic controls. J. Geophys. Res. **115**, D06111.

52) Crutzen, P.J. and Brühl, C. (1993) A model study of atmospheric temperatures and the concentrations of ozone, hydroxyl, and some other photochemically active gases during the glacial, the pre-industrial Holocene and the present. Geophys. Res. Lett. **20**, 1047–1050.

53) Martinerie, P., Brasseur, G.P. and Granier, C. (1995) The chemical composition of ancient atmospheres: A model study constrained by ice core data. J. Geophys. Res. **100**, 14291–14304.

54) Sowers, T., Alley, R.B. and Jubenville, J. (2003) Ice core records of atmospheric N_2O covering the last 106,000 years. Science **301**, 945–948.

55) Schilt, A., Brook, E.J., Bauska, T.K., Baggenstos, D., Fischer, H., Joos, F. *et al.* (2014) Isotopic constraints on marine and terrestrial N_2O emissions during the last deglaciation. Nature **516**, 234–237.

56) Keeling, C.D., Piper, S.C., Bacastow, R.B., Wahlen, M., Whorf, T.P., Heimann, M. *et al.* (2005) Atmospheric CO_2 and $^{13}CO_2$ exchange with the terrestrial biosphere and oceans from 1978 to 2000: Observations and carbon cycle implications. *In* A History of Atmospheric CO_2 and Its Effects on Plants, Animals, and Ecosystems (eds. Ehleringer, J.R., Cerling, T.E. and Dearing, M.D.). Springer Verlag, New York, pp. 83–113.

57) Nakazawa, T., Ishizawa, M., Higuchi, K. and Trivett, N.B.A. (1997) Two curve fitting methods applied to CO_2 flask data. Environmetrics **8**, 197–218.

58) Patra, P.K., Maksyutov, S., Ishizawa, M., Nakazawa, T., Takahashi, T. and Ukita, J. (2005) Interannual and decadal changes in the sea-air CO_2 flux from atmospheric CO_2 inverse modeling. Global Biogeochem. Cycles **19**, GB4013.

59) Rödenbeck, C., Bakker, D.C.E., Metzl, N., Olsen, A., Sabine, C., Cassar, N. *et al.* (2014) Interannual sea-air CO_2 flux variability from an observation-driven ocean mixed-layer scheme. Biogeosciences **11**, 4599–4613.

60) Nakazawa, T., Machida, T., Tanaka, M., Fujii, Y., Aoki, S. and Watanabe, K. (1993) Atmospheric CO_2 concentrations and carbon isotopic ratios for the last 250 years deduced from an Antarctic ice core, H15. *In* Proceedings of the 4th International Carbon Dioxide Conference. World Meteorological Organization, WMO/TD NO-361, Geneva,

pp. 193–196.
61) Machida, T., Nakazawa, T., Tanaka, M., Fujii, Y., Aoki, S. and Watanabe, O. (1994) Atmospheric CH_4 and N_2O concentrations during the last 250 years deduced from H15 ice core, Antarctica. *In* Proceedings of the 5th International Symposium on Global Cycles of Atmospheric Greenhouse Gases, Sendai, pp. 113–116.
62) Francey, R.J., Allison, C.E., Etheridge, D.M., Trudinger, C.M., Enting, I.G., Leuenberger, M. *et al.* (1999) A 1000-year high precision record of $\delta^{13}C$ in atmospheric CO_2. Tellus B **51**, 170–193.
63) Graven, H., Allison, C.E., Etheridge, D.M., Hammer, S., Keeling, R.F., Levin, I. *et al.* (2017) Compiled records of carbon isotopes in atmospheric CO_2 for historical simulations in CMIP6. Geosci. Model Dev. **10**, 4405–4417.
64) Nakazawa, T., Machida, T., Tanaka, M., Fujii, Y., Aoki, S. and Watanabe, O. (1993) Differences of the atmospheric CH_4 concentration between the Arctic and Antarctic regions in pre-industrial/pre-agricultural era. Geophys. Res. Lett. **20**, 943–946.
65) Chappellaz, J., Blunier, T., Kints, S., Daellenbach, A., Barnola, J.-M., Schwander, J. *et al.* (1997) Changes in the atmospheric CH_4 gradient between Greenland and Antarctica during the Holocene. J. Geophys. Res. **102**, 15987–15997.
66) Hodson, E.L., Poulter, B., Zimmermann, N.E., Prigent, C. and Kaplan, J.O. (2011) The El Niño-Southern Oscillation and wetland methane interannual variability. Geophys. Res. Lett. **38**, L08810.
67) Worden, J., Jiang, Z., Jones, D.B.A., Alvarado, M., Bowman, K., Frankenberg, C. *et al.* (2013) El Niño, the 2006 Indonesian peat fires, and the distribution of atmospheric methane. Geophys. Res. Lett. **40**, 4938–4943.
68) Dlugokencky, E.J., Masarie, K.A., Lang, P.M. and Tans, P.P. (1998) Continuing decline in the growth rate of the atmospheric methane burden. Nature **393**, 447–450.
69) Dlugokencky, E.J., Houweling, S., Bruhwiler, L., Masarie, K.A., Steele, L.P., Miller, J.B. *et al.* (2003) Atmospheric methane levels off: Temporary pause or a new steady-state? Geophys. Res. Lett. **30**, 1992.
70) Bousquet, P., Ciais, P., Miller, J.B., Dlugokencky, E.J., Hauglutaine, D.A., Prigent, C. *et al.* (2006) Contribution of anthropogenic and natural sources to atmospheric methane variability. Nature **443**, 439–443.
71) Nisbet, E.G., Dlugokencky, E.J., Manning, M.R., Lowry, D., Fisher, R.E., France, J.L. *et al.* (2016) Rising atmospheric methane: 2007–2014 growth and isotopic shift. Global Biogeochem. Cycles **30**, 1356–1370.
72) Morimoto, S., Fujita, R., Aoki, S., Goto, D. and Nakazawa, T. (2017) Long-term variations of the mole fraction and carbon isotope ratio of atmospheric methane observed at Ny-Ålesund, Svalbard from 1996 to 2013. Tellus B **69**, 1380497.
73) Patra, P.K., Saeki, T., Dlugokencky, E.J., Ishijima, K., Umezawa, T., Ito, A. *et al.* (2016) Regional methane emission estimation based on observed atmospheric concentrations (2002–2012). J. Meteorol. Soc. Jpn. **94**, 91–113.
74) Rigby, M., Montzka, S.A., Prinn, R.G., White, J.W.C., Young, D., O'Doherty, S. *et al.* (2017) Role of atmospheric oxidation in recent methane growth. Proc. Natl. Acad. Sci. U.S.A. **114**, 5373–5377.
75) Turner, A.J., Frankenberg, C., Wennberg, P.O. and Jacob, D.J. (2017) Ambiguity in the causes for decadal trends in atmospheric methane and hydroxyl. Proc. Natl. Acad. Sci. U.S.A. **114**, 5367–5372.
76) Thompson, R.L., Nisbet, E.G., Pisso, I., Stohl, A., Blake, D., Dlugokencky, E.J. *et al.* (2018) Variability in atmospheric methane from fossil fuel and microbial sources over the last three decades. Geophys. Res. Lett. **45**, 11499–11508.
77) Naus, S., Montzka, S.A., Pandey, S., Basu, S., Dlugokencky, E.J. and Krol, M. (2019) Constraints and biases in a tropospheric two-box model of OH. Atmos. Chem. Phys. **19**, 407–424.
78) Lelieveld, J., Dentener, F.J., Peters, W. and Krol, M.C. (2004) On the role of hydroxyl radicals in the self-cleansing capacity of the troposphere. Atmos. Chem. Phys. **4**, 2337–2344.
79) Voulgarakis, A., Naik, V., Lamarque, J.-F., Shindell, D.T., Young, P.J., Prather, M.J. *et al.* (2013) Analysis of present day and future OH and methane lifetime in the ACCMIP simulations. Atmos. Chem. Phys. **13**, 2563–2587.
80) Nevison, C.D., Dlugokencky, E., Dutton, G., Elkins, J.W., Fraser, P., Hall, B. *et al.* (2011) Exploring causes of interannual variability in the seasonal cycles of tropospheric nitrous oxide. Atmos. Chem. Phys. **11**, 3713–3730.
81) Saikawa, E., Schlosser, C.A. and Prinn, R.G. (2013) Global modeling of soil nitrous oxide emissions from natural processes. Global Biogeochem. Cycles **27**, 972–989.
82) Thompson, R.L., Chevallier, F., Crotwell, A.M., Dutton, G., Langenfelds, R.L., Prinn, R.G. *et al.* (2014) Nitrous oxide emissions 1999 to 2009 from a global atmospheric inversion. Atmos. Chem. Phys. **14**, 1801–1817.
83) Kondo, M., Patra, P.K., Sitch, S., Friedlingstein, P., Poulter, B., Chevallier, F. *et al.* (2020) State of the science in reconciling top-down and bottom-up approaches for terrestrial CO_2 budget. Glob. Change Biol. **26**, 1068–1084.
84) Francey, R.J., Tans, P.P., Allison, C.E., Enting, I.G., White, J.W.C. and Trolier, M. (1995) Changes in oceanic and terrestrial carbon uptake since 1982. Nature **373**, 326–330.
85) Goto, D., Morimoto, S., Ishidoya, S., Aoki, S. and Nakazawa, T. (2017) Terrestrial biospheric and oceanic CO_2 uptake estimated from long-term measurements of atmospheric CO_2 mole fraction, $\delta^{13}C$ and $\delta(O_2/N_2)$ at Ny-Ålesund, Svalbard. J.

Geophys. Res. Biogeosci. **122**, 1192–1202.
86) Keeling, R.F. and Shertz, S.R. (1992) Seasonal and interannual variations in atmospheric oxygen and implications for the global carbon cycle. Nature **358**, 723–727.
87) Tohjima, Y., Mukai, H., Nojiri, Y.U., Yamagishi, H. and Machida, T. (2008) Atmospheric O_2/N_2 measurements at two Japanese sites: Estimation of global oceanic and land biotic carbon sinks and analysis of the variations in atmospheric potential oxygen (APO). Tellus B **60**, 213–225.
88) Tohjima, Y., Mukai, H., Machida, T., Hoshina, Y. and Nakaoka, S. (2019) Global carbon budgets estimated from atmospheric O_2/N_2 and CO_2 observations in the western Pacific region over a 15-year period. Atmos. Chem. Phys. **19**, 9269–9285.
89) Ishidoya, S., Aoki, S., Goto, D., Nakazawa, T., Taguchi, S. and Patra, P.K. (2012) Time and space variations of the O_2/N_2 ratio in the troposphere over Japan and estimation of global CO_2 budget. Tellus B **64**, 18964.
90) Keeling, R.F. and Manning, A.C. (2014) Studies of recent changes in atmospheric O_2 content. *In* Treatise on Geochemistry (Second Edition) (eds. Holland, H.D. and Turekian, K.K.). Elsevier, Amsterdam, Vol. 5, pp. 385–404.
91) Gurney, K.R., Law, R.M., Denning, A.S., Rayner, P.J., Baker, D., Bousquet, P. *et al.* (2002) Towards robust regional estimates of CO_2 sources and sinks using atmospheric transport models. Nature **415**, 626–630.
92) Chevallier, F., Fisher, M., Peylin, P., Serrar, S., Bousquet, P., Bréon, F.-M. *et al.* (2005) Inferring CO_2 sources and sinks from satellite observations. Method and application to TOVS data. J. Geophys. Res. **110**, D24309.
93) Chevallier, F., Ciais, P., Conway, T.J., Aalto, T., Anderson, B.E., Bousquet, P. *et al.* (2010) CO_2 surface fluxes at grid point scale estimated from a global 21 year reanalysis of atmospheric measurements. J. Geophys. Res. **115**, D21307.
94) Patra, P.K., Maksyutov, S., Ishizawa, M., Nakazawa, T. and Inoue, G. (2005) Role of biomass burning and climate anomalies for land-atmosphere carbon fluxes based on inverse modeling of atmospheric CO_2. Global Biogeochem. Cycles **19**, GB3005.
95) Le Quéré, C., Rödenbeck, C., Buitenhuis, E.T., Conway, T.J., Langenfelds, R., Gomez, A. *et al.* (2007) Saturation of the Southern Ocean CO_2 sink due to recent climate change. Science **316**, 1735–1738.
96) Peylin, P., Law, R.M., Gurney, K.R., Chevallier, F., Jacobson, A.R., Maki, T. *et al.* (2013) Global atmospheric carbon budget: Results from an ensemble of atmospheric CO_2 inversions. Biogeosciences **10**, 6699–6720.
97) Saeki, T., Maksyutov, S., Saito, M., Valsala, V., Oda, T., Andres, R.J. *et al.* (2013) Inverse modeling of CO_2 fluxes using GOSAT data and multi-year ground-based observations. Sci. Online Lett. Atmos. **9**, 45–50.
98) van der Laan-Luijkx, I.T., van der Velde, I.R., van der Veen, E., Tsuruta, A., Stanislawska, K., Babenhauserheide, A. *et al.* (2017) The CarbonTracker Data Assimilation Shell (CTDAS) v1.0: Implementation and global carbon balance 2001–2015. Geosci. Model Dev. **10**, 2785–2800.
99) Palmer, P.I., Feng, L., Baker, D., Chevallier, F., Bösch, H. and Somkuti, P. (2019) Net carbon emissions from African biosphere dominate pantropical atmospheric CO_2 signal. Nat. Commun. **10**, 3344.
100) Gaubert, B., Stephens, B.B., Basu, S., Chevallier, F., Deng, F., Kort, E.A. *et al.* (2019) Global atmospheric CO_2 inverse models converging on neutral tropical land exchange, but disagreeing on fossil fuel and atmospheric growth rate. Biogeosciences **16**, 117–134.
101) Stephens, B.B., Gurney, K.R., Tans, P.P., Sweeney, C., Peters, W., Bruhwiler, L. *et al.* (2007) Weak northern and strong tropical land carbon uptake from vertical profiles of atmospheric CO_2. Science **316**, 1732–1735.
102) Saeki, T. and Patra, P.K. (2017) Implications of overestimated anthropogenic CO_2 emissions on East Asian and global land CO_2 flux inversion. Geosci. Lett. **4**, 9.
103) Fujita, R., Morimoto, S., Maksyutov, S., Kim, H.-S., Arshinov, M., Brailsford, G. *et al.* (2020) Global and regional CH_4 emissions for 1995–2013 derived from atmospheric CH_4, δ^{13}C-CH_4, and δD-CH_4, observations and a chemical transport model. J. Geophys. Res. **125**, e2020JD032903.
104) Hirsch, A.I., Michalak, A.M., Bruhwiler, L.M., Peters, W., Dlugokencky, E.D. and Tans, P.P. (2006) Inverse modeling estimates of the global nitrous oxide surface flux from 1998–2001. Global Biogeochem. Cycles **20**, GB1008.
105) Huang, J., Golombeck, A., Prinn, R., Weiss, R., Fraser, P., Simmonds, P. *et al.* (2008) Estimation of regional emissions of nitrous oxide from 1997 to 2005 using multinetwork measurements, a chemical transport model, and an inverse method. J. Geophys. Res. **113**, D17313.
106) Saikawa, E., Prinn, R.G., Dlugokencky, E., Ishijima, K., Dutton, G.S., Hall, B.D. *et al.* (2014) Global and regional emissions estimates for N_2O. Atmos. Chem. Phys. **14**, 4617–4641.
107) Thompson, R.L., Ishijima, K., Saikawa, E., Corazza, M., Karstens, U., Patra, P.K. *et al.* (2014) TransCom N_2O model inter-comparison, Part II: Atmospheric inversion estimates of N_2O emissions. Atmos. Chem. Phys. **14**, 6177–6194.
108) Thompson, R.L., Lassaletta, L., Patra, P.K., Wilson, C., Wells, K.C., Gressent, A. *et al.* (2019) Acceleration of global N_2O emissions seen from two decades of atmospheric inversion. Nat. Clim. Chang. **9**, 993–998.
109) Sykila, A. and Kroeze, C. (2011) The global nitrous oxide budget revisited. Greenh. Gas Meas. Manage. **1**, 17–26.
110) Davidson, E.A. and Kanter, D. (2014) Inventories

and scenarios of nitrous oxide emissions. Environ. Res. Lett. **9**, 105012.
111) Tian, H., Yang, J., Lu, C., Xu, R., Canadell, J.G., Jackson, R. *et al.* (2018) The global N_2O Model Intercomparison Project (NMIP): Objectives, simulation protocol and expected products. Bull. Am. Meteorol. Soc. **99**, 1231–1251.

(Received Jan. 5, 2020; accepted Aug. 31, 2020)

Profile

Takakiyo Nakazawa was born in 1947 in Shimane Prefecture. He is currently a professor emeritus at Tohoku University, where he has also served on the Faculty of Science/Graduate School of Science as an assistant professor, an associate professor, a professor and a visiting professor. He also served as a visiting researcher at the Scripps Institution of Oceanography, a visiting associate professor at the Institute of Space and Astronautical Science and the National Institute of Polar Research, a leader of the Greenhouse Gases Modeling Group at the Frontier Research Center for Global Change, and a visiting senior scientist of the Environmental Biogeochemical Cycles Research Program at the Japan Agency for Marine-Earth Science and Technology. His work has focused on elucidating the global cycling of greenhouse gases based on observations and modeling, after studying the light absorption properties of the atmospheric components. For these achievements, he was awarded the Award of the Meteorological Society of Japan, Yamazaki Award, Nissan Science Prize, Miyake Award, Shimadzu Award, Medal with Purple Ribbon, and Fujiwhara Award, and he was recognized as a Japan Geoscience Union Fellow.